NASA TECHNICAL NOTE

NASA TN D-2731

NASA TN D-2731

AMPTIAC

59653

DISTRIBUTION STATEMENT A
Approved for Public Release
Distribution Unlimited

PERFORMANCE OF SEVEN SEMICIRCULAR LIFT-PRODUCING NOZZLES

by Charles J. Shoemaker

Langley Research Center
Langley Station, Hampton, Va.

20011130 152

NATIONAL AERONAUTICS AND SPACE ADMINISTRATION • WASHINGTON, D. C. • APRIL 1965

NASA TN D-2731

PERFORMANCE OF SEVEN SEMICIRCULAR LIFT-PRODUCING NOZZLES

By Charles J. Shoemaker

Langley Research Center
Langley Station, Hampton, Va.

**Reproduced From
Best Available Copy**

NATIONAL AERONAUTICS AND SPACE ADMINISTRATION

For sale by the Office of Technical Services, Department of Commerce,
Washington, D.C. 20230 -- Price $2.00

PERFORMANCE OF SEVEN SEMICIRCULAR LIFT-PRODUCING NOZZLES

By Charles J. Shoemaker
Langley Research Center

SUMMARY

An investigation of the thrust coefficient and lift force produced by seven semicircular lift-producing nozzles was conducted with air at ratios of total pressure to ambient pressure up to 1000. The nozzle-exit Mach numbers ranged from 2.22 to 4.54. The models were originally circular cross-section nozzles designed by the method of characteristics for uniform axial flow at the exit. These circular nozzles were split and a flat plate substituted for the lower half. The models were further modified to produce lift by cutting notches in the trailing edge of the flat plate. Test results of each configuration are given. Notching the flat plate did not significantly affect the thrust coefficient. A lift-thrust ratio of 0.21 was the maximum value recorded.

INTRODUCTION

Throughout the range of flight speeds, aircraft can advantageously use an increase in lift. Improvements in low-speed lift can be used to reduce take-off distances. During cruise higher lift could be used to increase the payload. If the lift-drag ratio is also increased the range can be improved. At high altitudes where aerodynamic controls become ineffective, lift forces can be used for directional control.

One method of increasing lift is to deflect the exhaust of a jet engine. Several jet deflection devices such as swiveled nozzles, movable plugs, and flaps are compared in reference 1. Reference 2 reports the lift force obtained from sonic nozzles that have an oblique exit plane (skewed). For attitude control of a rocket, reference 3 presents the steering moment of asymmetric "pen-shape" nozzles that form the trailing edge of a canard. A different asymmetric nozzle which has an opening in the surface through which part of the flow expands is the subject of this report.

Originally the test nozzles were axially symmetric and were designed by the method of characteristics for uniform axial flow at the exit. These nozzles were split longitudinally and a flat plate substituted for the lower half. The nozzles were further modified to produce lift by cutting notches in the trailing edge of the flat plate. Test results are given for each stage of the modifications. The nozzle ambient pressures ranged from 14.7 to 0.5 psia. Ratios of total pressure to ambient pressure up to 1000 were

used. Maximum total pressure was about 515 psia, and total temperature was approximately 530° R.

SYMBOLS

A_N area of notch, sq in.

A^* nozzle throat area, sq in.

C_T coefficient of thrust, $T/p_t A^*$

F_L force in lift direction, lb (see eq. (B1))

F_T thrust force computed from nozzle pressure, lb (see eq. (A1))

L lift, lb

L_c lift calculated from nozzle parameters, lb

M Mach number

$\Delta M = \dfrac{M_{design} - M_{cutoff}}{M_{design}}$

M_L lift force moment, in-lb

M_T moment computed from nozzle parameters, in-lb

$\dot{m}$ mass flow, $\dfrac{\text{lb-sec}}{\text{ft}}$

p_s separation pressure, psia

p_t total pressure, psia

p_w wall static pressure, psia

p_∞ ambient pressure, psia

$p_{\infty,av}$ average value of ambient pressure for each test

p^* nozzle throat static pressure, psia

r nozzle radius, in.

r_e nozzle exit radius, in.

r^* nozzle throat radius, in.

T thrust, lb

V^* velocity at nozzle throat, ft/sec

x axial distance from nozzle throat, in.

x_e nozzle exit station

x^* nozzle throat station

$\bar{x}_L$ centroid of action of lift, in.

y distance perpendicular to nozzle X-axis, in.

$\bar{y}_T$ location of eccentric thrust above flat plate, in.

θ the angle between radius and flat plate at a station, rad

APPARATUS

Test Section and Air Supply

A photograph showing the general arrangement of the test section with a nozzle in place is given in figure 1, and a detailed drawing of the test section is presented in figure 2. The sidewalls of the test section contain movable windows of schlieren quality glass. The air supply pipes within the test section are also used to support the nozzle.

Static pressure within the test section could be varied from 14.7 to 0.5 psia by exhausting the test section into the intake of a high-capacity compressor. Bypass valves to the compressor intake provided coarse adjustment of the test-section pressure. Final regulation of the pressure was obtained with a bleed valve in the duct downstream of the test section.

Nozzle Design

Circular nozzles.- The basic circular-cross-section nozzles were designed with the use of a computer program based on the three-dimensional characteristics method of reference 4. These nozzles were designed to have a minimum length with axial flow at the exit. The minimum length restriction on the design gives a sharp corner at the throat. This corner was rounded slightly to give a smooth transition from the converging to diverging portion of the nozzle. The nozzle inviscid contours were not corrected for boundary-layer growth. Seven nozzles were made that had exit Mach numbers ranging from 2.22

to 4.54. Internal coordinates for each nozzle are given in table I and a typical circular nozzle is shown in figure 3.

Semicircular nozzles.- The circular nozzles were split longitudinally and a flat plate substituted for one-half of each nozzle to make semicircular nozzles. (See fig. 4.) Symmetry of the characteristic network about the nozzle center line permits substitution of the flat plate without changing the inviscid network or pressure distribution. However, the thrust would be reduced to one-half the value of that for the circular nozzle because of the reduction in mass flow.

Lift-producing modifications.- The lift-producing modifications are based on the fact that any disturbance in the flow originating on the flat plate and located downstream of the last characteristic line cannot propagate to the opposite wall. Therefore, notches can be cut in the trailing edge of the flat plate as deep as the last characteristic line and not change the wall-static-pressure distribution or thrust. For inviscid flow, when the nozzle is operating at design pressure ratio (nozzle exit pressure equals ambient pressure) air would not expand through the notch and there is no lift force. However, when the nozzle exit pressure is greater than the ambient pressure (under expanded), air would expand through the notch and give a lift force, without changing the pressure distribution or thrust.

The semicircular nozzles had V-notches cut into the trailing edge of the flat plate up to the last characteristic line of the inviscid characteristic network. These V-notches are identified by the value of the ratio of the notch depth divided by the depth of the apex of the V (cone) formed by the last characteristic line - for example, 3/3.

Another type of notch was cut in the trailing edge of the flat plate to determine how much of the flat plate could be removed before the thrust was reduced. These notches were cut along straight-line approximations of constant Mach number contours which were obtained from the inviscid characteristic computations. These notches are identified by the Mach number ratio

$$\Delta M = \frac{M_{design} - M_{cutoff}}{M_{design}}$$

Throughout this report these notches are referred to as ΔM notches.

Figure 5 gives the coordinates and semiplan of all the notches used in this investigation. The upper contour shown for each nozzle is the intersection of the internal surface of the split nozzle and flat plate. Figure 6 shows the deepest notch (ΔM = 30 percent) cut into the flat plate of nozzle 7 (M = 4.54).

Instrumentation

Thrust.- Nozzle thrust was indicated by strain gages bonded to each end of the two vertical air supply pipes connected to the settling chamber in the test

section. (See fig. 2.) The thrust gages were calibrated by pulling on the settling chamber with calibrated weights up to a maximum of 300 pounds for the circular nozzles and a maximum of 150 pounds for the semicircular nozzles. During a test run, thrust was continuously recorded as a function of nozzle total pressure by an electronic x-y plotter. The accuracy of the thrust is estimated to be ±2.5 percent of full-scale value.

The theoretical position of the eccentric thrust of the semicircular nozzles was calculated by using the nozzle-internal-pressure distribution by the method given in appendix A.

Lift.- The lift force was measured by strain gages bonded on two aluminum-alloy tension beams. A drawing of a tension beam is shown in figure 7 and a photograph of the beam mounted in the test section is shown in figure 8. The wall attaching points were designed to prevent bending of the tension beam when the nozzle support pipe moved a few thousandths of an inch due to thrust. Lateral restraint was provided by a set of turnbuckles connected to the side walls. There was no detectable change in the thrust calibration when these lateral restraints were in place.

The upper and lower tension beams were balanced electrically to give equal deflection on the lift recorder for identical loads. Then the beams were installed in the test section with about 45 pounds tension in each beam when the model support pipe was centered in the test section. The strain gages were interconnected to indicate lift by the difference in tension in the beams.

The lift tension beams were calibrated with loads up to 30 pounds at three lift locations to account for changes in lift position due to nozzle changes. For each nozzle the theoretical location of the lift force was calculated from the wall static pressures by using the procedure of appendix B.

The interaction of eccentric thrust on the lift data was determined by applying thrust loads of known eccentricity. The thrust measured during a test and the calculated eccentric thrust position (appendix A) were used to remove the thrust interaction from the lift data.

Lift was recorded on an electronic x-y plotter as a function of the nozzle total pressure. The estimated accuracy of the lift data is ±2.5 percent of the maximum value.

Pressure measurements.- Total pressure in the settling chamber was measured by a 500-psi pressure transducer. This transducer had an accuracy of ±2.5 psi.

Four of the semicircular nozzles were instrumented with static orifices on the internal surfaces as shown in figure 9. Orifice number 9 on the flat plate of nozzle 6 was removed when the notch was enlarged from 3/3 to ΔM = 10 percent.

Schlieren.- Schlieren photographs were taken with a double-pass system by using the flash from a mercury-arc light source. Alinement and proportions of the jet plume may be scaled by comparison with a wire grid having 3-inch squares which was fastened to the window frame.

RESULTS AND DISCUSSION

Thrust Coefficient

The variation of thrust coefficient with the ratio of total pressure to ambient pressure for the circular and semicircular nozzles is given in figures 10 and 11. Theoretical inviscid thrust coefficients are indicated by the dashed lines starting at the nozzle design p_t/p_∞ and extending to the maximum value for the test. Above the design pressure ratio, the ratio of measured thrust coefficient to inviscid thrust coefficient is about 0.98. Data with total pressures less than 100 psia have been omitted because of accuracy considerations.

Effect of nozzle shape.- Comparison of the faired data of figures 10 and 11 reveals that the measured thrust coefficients for the semicircular nozzles are generally slightly greater than the measured thrust coefficients for the circular nozzles under comparable conditions. The greater value of the measured thrust coefficient for the semicircular nozzles is not a true aerodynamic effect but is attributed to experimental error in the measurements made with the circular nozzles and with lateral restraints not employed. In no instance, however, does the measured thrust coefficient of a semicircular nozzle exceed by more than 2 percent the value observed for the corresponding circular nozzle at comparable operating conditions. Within the accuracy of the data the values of the thrust coefficients for the semicircular nozzles are regarded as indistinguishable from the values for the corresponding circular nozzles.

Effect of notches.- The semicircular configuration with a solid flat plate was used as a reference to determine the effect of notching the flat plate on the thrust coefficient. Figure 12 presents faired curves showing the range of thrust coefficient for each nozzle with all its notch configurations. The fairings are for data with a total pressure equal to or greater than 100 psia and with at least design pressure ratio. The range of the thrust coefficients about the no-notch line is ±2.5 percent which is the accuracy of the thrust data. In general, within the accuracy of the data, notches in the flat plate did not appear to affect the thrust coefficients.

The reduction in friction force due to notching the flat plate was estimated for the 3/3 notch of nozzle 7 by using the friction coefficient from figure 19 of reference 5. This force was slightly less than 0.2 pound which is too small to be detected in the thrust data.

Lift

A theoretical inviscid lift force was calculated from the sum of the internal and external forces acting on the nozzle. The lift force is expressed by the following relation:

$$L_c = \Sigma F_L - A_N p_\infty \qquad (1)$$

where ΣF_L is the sum of the internal forces acting on the nozzle surface in the lift direction. These forces are evaluated by the method described in appendix B and the values of ΣF_L are given in table II. The term $A_N p_\infty$ is

the sum of the external forces acting on the nozzle in the lift direction. Values of the notch area A_N are also given in table II.

Lift-thrust ratio.- The experimental values of lift-thrust ratio are given in figure 13 as a function of total-to-ambient pressure ratio. At the nozzle design pressure ratio, the lift-thrust ratio is larger than zero because the nozzle contours were not corrected for boundary-layer displacement thickness which effectively reduces the nozzle expansion ratio and gives higher surface pressures which increase the lift force. The lift-thrust ratio increases as the total-to-ambient pressure ratio becomes larger. Increasing the notch area of a nozzle also raises the lift-thrust ratio except for nozzle 7 with the ΔM = 30 percent notch. For this case lift oscillations occurred when the total-to-ambient pressure ratio was less than 405.

A maximum lift-thrust ratio of 0.21 was obtained from nozzle 5 with the ΔM = 20 percent notch. The corresponding thrust coefficient is 1.57 for this nozzle-notch combination. In order to give the same horizontal thrust and lift, a gimbaled nozzle would require a thrust coefficient of approximately 1.60 and would have to be directed 11.8° downward.

The faired curves for the V-notches of figure 13 are replotted in figure 14. Included in the figure are the inviscid lift-thrust ratios. Experimental lift-thrust ratios are larger than the inviscid values because the experimental lift is greater than the inviscid value due to the previously mentioned boundary-layer effect and the experimental thrust is less than the inviscid value which, when divided into the lift, increases the ratio. The general trend of the data is for the lift-thrust ratio of the V-notches to decrease as the exit Mach number of the nozzle increases.

Flow Separation

Although the main concern of this investigation was with nozzle underexpanded flow, a limited quantity of longitudinal pressure gradient data for separated flow during the regions of overexpanded flow was obtained for the four nozzles shown in figure 9. An example of a plot used to determine separation pressure is given in figure 15 for nozzle 6 with a ΔM = 10 percent notch. With decreasing total-to-ambient pressure ratios the nozzle internal wall static pressure is proportional to the total pressure until separation occurs, then the slope of the curve changes. The separation pressure was read at the intersection of the two portions of the wall static plot. Figure 16 gives the separation-to-total pressure ratio as a function of the total-to-ambient pressure ratio. Part (a) of the figure shows the separation pressures along the top center line of the nozzle semicircular surface, whereas part (b) gives the separation pressures at other positions on the internal surface of the nozzle. For comparison purposes the separation pressure data obtained from references 6 and 7 for conical nozzles are included.

Note that the semicircular-nozzle flow separated at pressures slightly less than ambient pressure; this suggests laminar flow. If the criterion that boundary-layer transition occurs at a Reynolds number based on momentum thickness of 1000 is used, a rough estimation of the pressure ratio at transition

was made with the assumption that the nozzle could be replaced with a cylinder that has constant flow properties equal to the midlength of the nozzle. This estimation indicated that transition occurred at pressure ratios greater than the design value for all the nozzles except nozzles 6 and 7; therefore, laminar boundary layers occurred for most of the test. The conical nozzles of references 6 and 7 are 4 to 6 times longer than nozzle 7 which would give them a turbulent boundary layer and consequently lower separation pressures.

Schlieren Photographs

Typical schlieren photographs of the exhaust plume of the nozzle configurations and various notches are presented in figure 17. Part (a) depicts the exhaust plume of nozzle 4 for the circular, semicircular solid flat plate, and semicircular 3/3 notch configurations. Although not shown, the exhaust plume of the semicircular nozzle with the flat plate perpendicular to the schlieren light path was similar to the circular configuration shown. Part (b) of the figure shows the exhaust plume of nozzle 7 with the ΔM = 10 percent and ΔM = 30 percent notches. The photographs of nozzle 4 with the 3/3 notch show no expansion through the notch until the pressure ratio is greater than the design value. However, for nozzle 7, the flow did expand through the ΔM = 10 percent and ΔM = 20 percent notches at pressure ratios less than design value.

CONCLUSIONS

An experimental investigation was conducted to determine the lift and thrust characteristics of seven semicircular nozzles with exit Mach numbers ranging from 2.22 to 4.54. Lift was obtained by operating at higher than design pressure ratios with part of the airflow discharging in a downward direction through various size notches cut in the trailing edge of a flat plate forming one boundary of the semicircular shape. The following results were obtained:

1. In general, the lift-thrust ratio of a nozzle increased with notch size except for the largest notch investigated which gave a reduction in the lift-thrust ratio.

2. A maximum value of lift-thrust ratio of 0.21 was obtained with a Mach 3.76 nozzle which had a notch extending upstream of the last Mach cone in the characteristics network.

3. Experimental values of lift-thrust ratios were larger than theoretical inviscid values because the measured thrust was smaller than theoretical thrust and the measured lift was larger than theoretical lift due to boundary-layer displacement effects.

4. Within the accuracy of the data the flow through the notches did not appear to affect the thrust coefficient significantly.

5. Schlieren photographs show that no air flowed through notches cut up to the boundaries of the last characteristic cone when the internal pressure at the nozzle exit was equal to the ambient pressure.

Langley Research Center,
National Aeronautics and Space Administration,
Langley Station, Hampton, Va., November 23, 1964.

APPENDIX A

ECCENTRIC THRUST POSITION

The position of the thrust force above the center line of the model support pipe was calculated by using an analytical thrust and moment which are described in this appendix.

The analytical thrust was computed with the use of the following relation:

$$F_T = \int_{r^*}^{r_e} r \int_0^{\pi} \left(p_w - p_\infty\right) d\theta \, dr + \dot{m}V^* + \left(p^* - p_\infty\right) \frac{\pi r^{*2}}{2} \tag{A1}$$

which is the sum of the horizontal forces and momentum terms between the settling chamber and the nozzle exit. In evaluating equation (A1) the throat parameters (p^*, $\dot{m}$, V^*) were assumed to be the inviscid design values.

Limited static pressure data from this investigation indicate that V-notches as deep as the last characteristic line do not have wall circumferential pressure gradients and that the internal pressures are nearly the inviscid values. Therefore, the inviscid pressures were used for all the V-notch configurations.

The ΔM notch data indicate that upstream of the edge of the notch the wall circumferential pressure is uniform and is nearly equal to the inviscid pressure. Downstream of the notch edge there is a pressure gradient which was evaluated from the data.

The analytical moment was obtained by use of the following equation:

$$M_T = \int_{r^*}^{r_e} r^2 \int_0^{\pi} \left(p_w - p_\infty\right) \sin\theta \, d\theta \, dr + \left[\dot{m}V^* + \left(p^* - p_\infty\right)\frac{\pi r^{*2}}{2}\right]\frac{4}{3\pi} r^* \tag{A2}$$

which is the horizontal forces multiplied by their respective moment arms.

The eccentric thrust axis is above the center line of the model support pipe by the distance $\overline{y}_T$ given in the following equation:

$$\overline{y}_T = \frac{M_T}{F_T} \tag{A3}$$

APPENDIX A

The eccentric thrust position was evaluated over the range of experimental total-to-ambient pressure ratios for each semicircular lift-producing nozzle. As the total-to-ambient pressure ratio is increased $\overline{y}_T$ initially increases but becomes nearly constant at large pressure ratios.

APPENDIX B

LOCATION OF LIFT FORCE

The vertical forces on the nozzle surfaces were combined into a single force that gave the same moment about the nozzle throat. The total force and moment on the nozzle semicircular surface and flat plate were evaluated separately, then combined to give the lift position.

Semicircular Surface

The force in the lift direction acting on the semicircular surface was evaluated from the static-pressure distribution by use of the following equation:

$$F_L = 2 \int_{x^*}^{x_e} \int_0^{\frac{\pi}{2}} r\left(p_w - p_\infty\right) \sin \theta \, d\theta \, dx \qquad (B1)$$

Equation (B1) reduces to the following form for the V-notches because they have no circumferential pressure gradient:

$$F_L = 2 \int_{x^*}^{x_e} r\left(p_w - p_\infty\right) \, dx$$

The accuracy of the ΔM notch calculations was limited by the small number of pressure orifices alined circumferentially at a station. (See fig. 9.) A sine curve seemed to fit the pressure distributions at stations with three orifices; therefore, all the circumferential pressure data were faired with similar curves.

Multiplying equation (B1) by the axial distance from the throat (x) gives the moment about the nozzle throat as shown in the following equation:

$$M_L = 2 \int_{x^*}^{x_e} x \int_0^{\frac{\pi}{2}} r\left(p_w - p_\infty\right) \sin \theta \, d\theta \, dx \qquad (B2)$$

APPENDIX B

Flat Plate

The circular nozzle has a radial pressure gradient about the center line at all stations but the throat and exit. When the nozzle is split and a flat plate added, the plate is subjected to this pressure gradient. The vertical force on the flat plate was obtained by integrating the pressures over the surface of the plate which gives the following relation:

$$F_L = -2 \int_{x^*}^{x_e} \int_0^r \left(p_w - p_\infty\right) dr\, dx \tag{B3}$$

Multiplying equation (B3) by the moment arm from the throat gives the moment which is:

$$M_L = -2 \int_{x^*}^{x_e} x \int_0^r \left(p_w - p_\infty\right) dr\, dx \tag{B4}$$

Lift Position

The summation of moments on the semicircular surface and flat plate was done in such a way that only the total moment due to lift was evaluated. This procedure was used because the nozzle is inherently subject to a moment due to the different pressure distributions on the semicircular surface and flat plate. Thus,

$$\Sigma M_L = \left[\left(M_L\right)_{\text{with notch}} - \left(M_L\right)_{\text{no notch}}\right]_{\text{semicircular}} + \left[\left(M_L\right)_{\text{with notch}} - \left(M_L\right)_{\text{no notch}}\right]_{\text{plate}} \tag{B5}$$

For the V-notches, equation (B5) reduces to the moment on the notch area prior to cutting the notch.

The location of the equivalent lift vector downstream of the nozzle throat was obtained as follows:

$$\bar{x}_L = \frac{\Sigma M_L}{\Sigma F_L} \tag{B6}$$

where ΣF_L is the sum of the force on the semicircular surface and the flat plate.

For the V-notches the lift position is constant and at the centroid of the notch area. The theoretical lift position of the ΔM notches is initially near the throat at the design total-to-ambient pressure ratio, then it moves downstream with increasing pressure ratio.

REFERENCES

1. Von Glahn, U. H.; and Povolny, J. H.: Considerations of Some Jet-Deflection Principles for Directional Control and for Lift. SAE Trans., vol. 66, 1958, pp. 620-629.

2. Carter, David J., Jr.; and Vick, Allen R.: Experimental Investigation of Axial and Normal Force Characteristics of Skewed Nozzles. NACA TN 4336, 1958.

3. Cubbison, Robert W.: Asymmetric "Penshape" Nozzles in Jet-Canard Configurations for Attitude Control. NASA TN D-1561, 1963.

4. Ferri, Antonio: Elements of Aerodynamics of Supersonic Flows. The Macmillan Co., 1949.

5. Matting, Fred W.; Chapman, Dean R.; Nyholm, Jack R.; and Thomas, Andrew G.: Turbulent Skin Friction at High Mach Numbers and Reynolds Numbers in Air and Helium. NASA TR R-82, 1961.

6. Farley, John M.; and Campbell, Carl E.: Performance of Several Method-of-Characteristics Exhaust Nozzles. NASA TN D-293, 1960.

7. Campbell, C. E.; and Farley, J. M.: Performance of Several Conical Convergent-Divergent Rocket-Type Exhaust Nozzles. NASA TN D-467, 1960.

TABLE I

NOZZLE INTERNAL COORDINATES

x, in.	r, in., for -						
	Nozzle 1 (M = 2.22)	Nozzle 2 (M = 2.63)	Nozzle 3 (M = 3.10)	Nozzle 4 (M = 3.41)	Nozzle 5 (M = 3.76)	Nozzle 6 (M = 4.02)	Nozzle 7 (M = 4.54)
0.0000	0.3535	0.3535	0.3535	0.3535	0.3535	0.3535	0.3535
.0354	.3570	.3588	.3606	.3613	.3620	.3634	.3648
.0707	.3623	.3659	.3694	.3712	.3729	.3747	.3782
.1414	.3747	.3818	.3889	.3924	------	------	------
.2475	------	------	------	.4260	.4348	.4390	.4454
.2828	.3995	.4171	.4277	------	------	------	------
.4242	.4242	.4489	------	------	------	------	------
.5303	------	------	.4984	.5161	.5331	.5444	.5621
.5656	.4461	.4790	------	------	------	------	------
.7070	.4638	.5048	------	------	------	------	------
.8838	------	------	.5833	.6116	.6416	.6610	.6936
.9191	.4850	.5380	------	------	------	------	------
1.1312	.4977	.5649	------	------	------	------	------
1.2373	------	------	.6469	.6893	.7317	.7593	.8081
1.3433	.5027	.5840	------	------	------	------	------
1.5625	.5041	------	------	------	------	------	------
1.5908		.6002	.6929	.7494	.8053	.8420	.9064
1.9443		.6087	.7247	.7954	------	------	------
2.1210		------	------	------	.8901	.9403	1.0294
2.2164		.6108	.7441	------	------	------	------
2.2978			------	.8290	------	------	------
2.6513			------	------	.9509	1.0145	1.1277
2.8280			.7600	.8618	------	------	------
3.1815			------	------	.9916	1.0729	1.2083
3.1833			.7607	------	------	------	------
3.3583				.8748	------	------	------
3.8885				------	1.0252	1.1213	1.2903
4.0052				.8838	------	------	------
4.5955					1.0393	1.1517	1.3539
5.1081					1.0393	------	------
5.4793						1.1666	1.4069
6.0590						1.1694	------
6.1863							1.4352
6.8933							1.4522
7.6003							1.4592
8.3497							1.4617

TABLE II

NOZZLE PARAMETERS

Nozzle	Notch	$\Sigma F_L/p_t$, sq in.	A_N, sq in.
1	1/3	0.01544	0.1688
2	2/3	0.02891	0.6047
3	1/3	0.01347	0.5660
	2/3	.02691	1.1312
	3/3	.04038	1.6972
4	1/3	0.01271	0.8493
	2/3	.02543	1.6987
	3/3	.03814	2.5478
	$\Delta M = 5\%$	[a].0672	3.7674
5	3/3	0.03589	3.9230
	$\Delta M = 10\%$	[b].0736	6.6220
	$\Delta M = 20\%$	[a].0736	7.5392
6	1/3	0.01145	1.7763
	2/3	.02291	3.5526
	3/3	.03432	5.3226
	$\Delta M = 10\%$	[a].0608	8.8704
7	3/3	0.03175	9.5658
	$\Delta M = 10\%$	[b].0560	15.5860
	$\Delta M = 20\%$	[a].0688	17.6040
	$\Delta M = 30\%$	[a].0736	18.6324

[a]Obtained from measured static pressures.
[b]Estimated values.

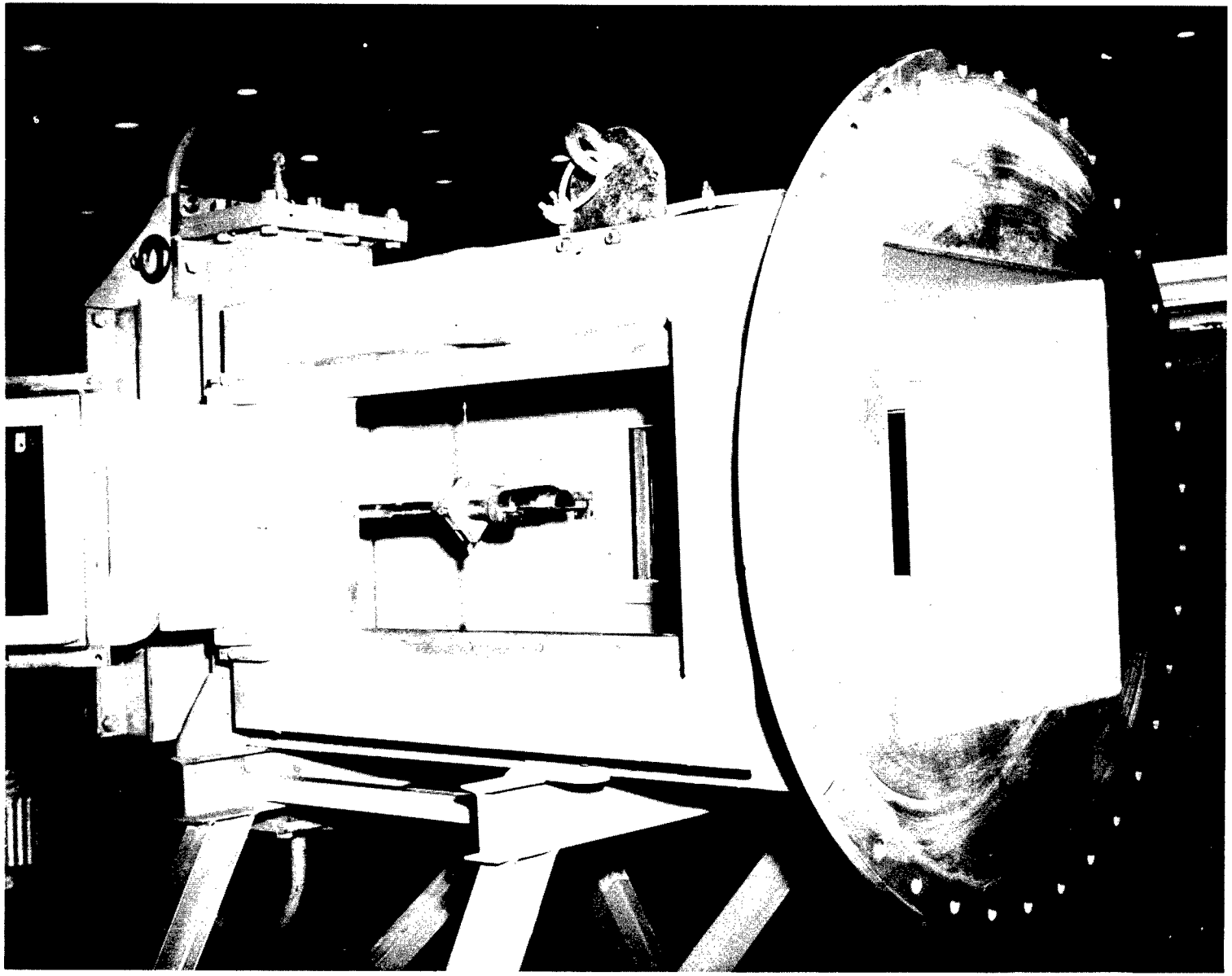

Figure 1.- Photograph of test section. L-64-7902

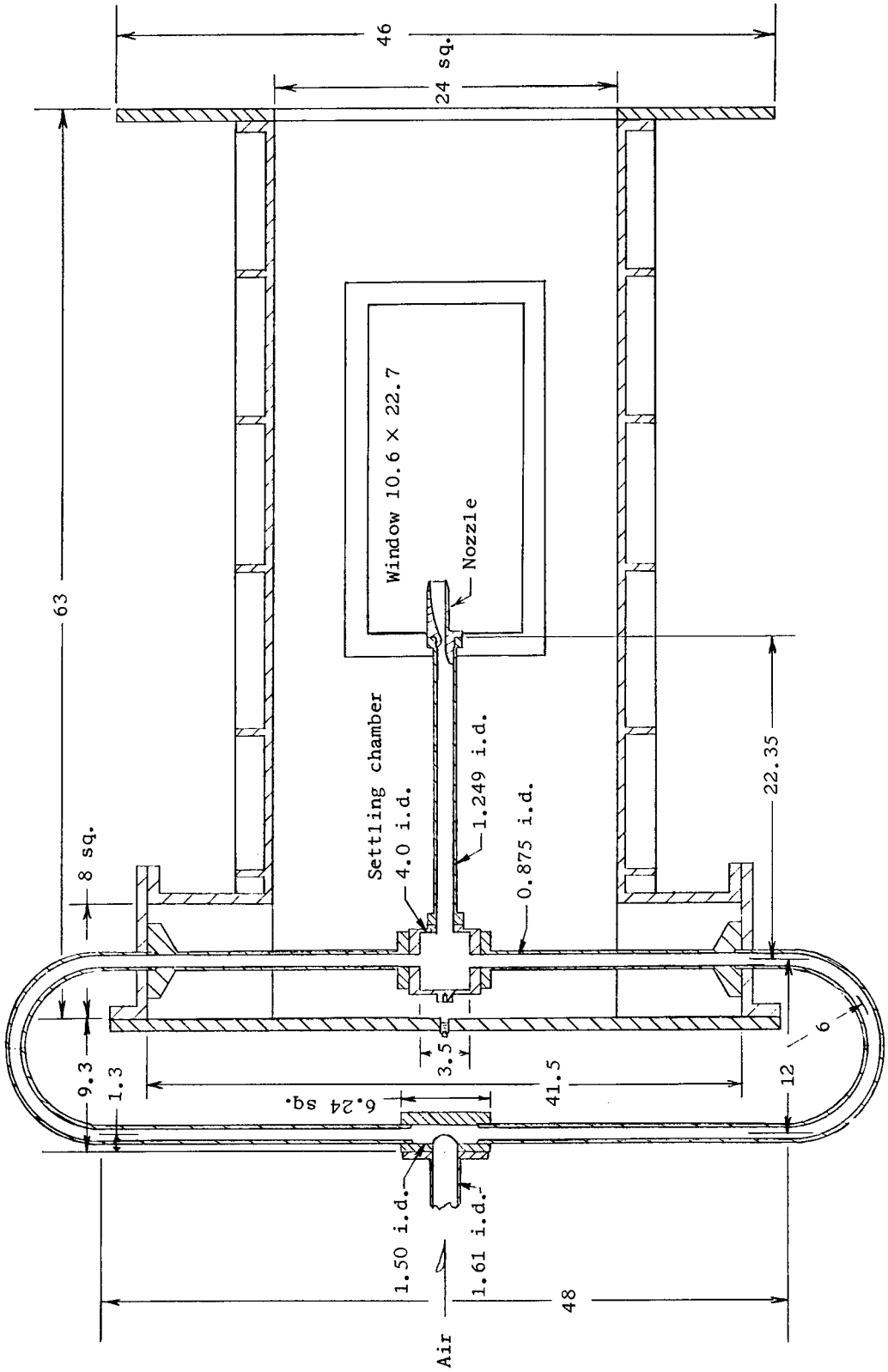

Figure 2.- Test section. All dimensions are in inches.

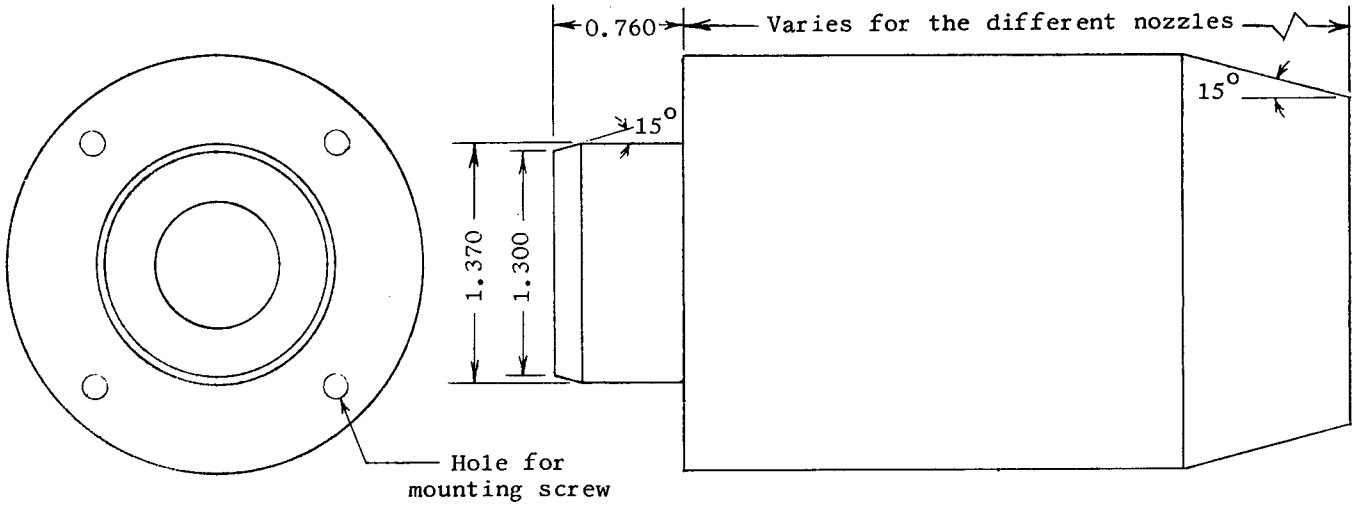

x, in.	y, in.
-.5430	.6250
-.5200	.5469
-.4900	.5080
-.4500	.4724
-.3000	.3987
-.1500	.3640
0.0000	.3535

(The coordinates downstream of the throat are given in table I.)

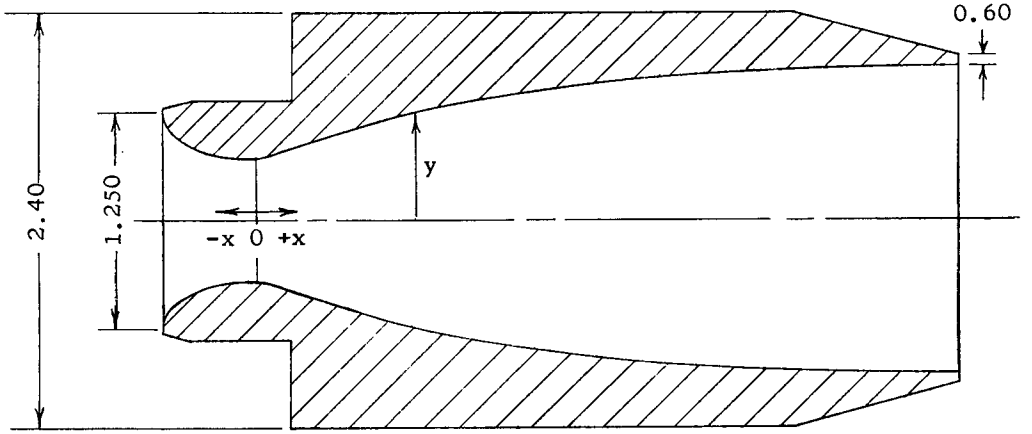

Figure 3.- General arrangement of the circular nozzles. All dimensions are in inches.

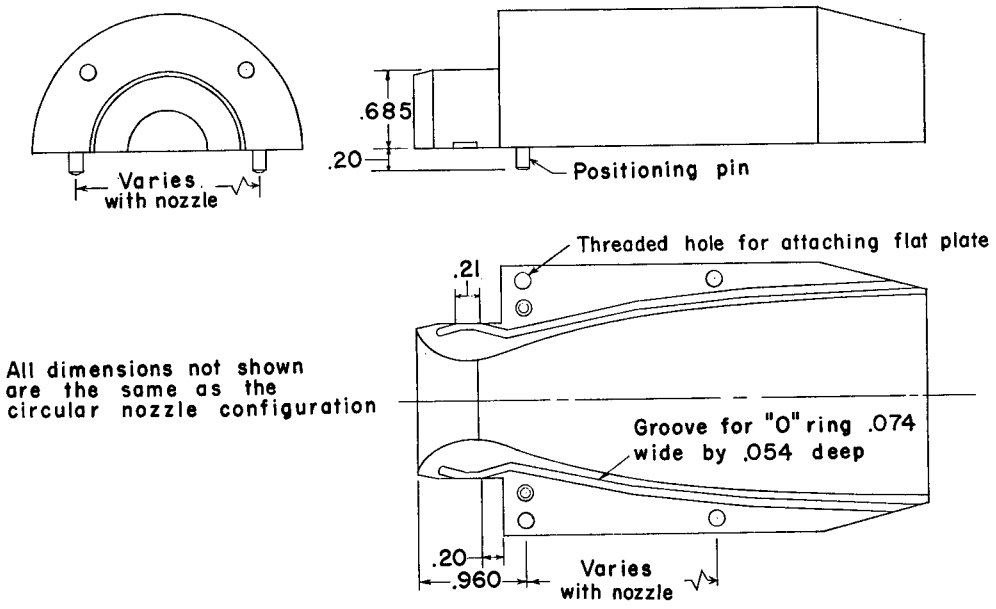

(a) Split nozzle.

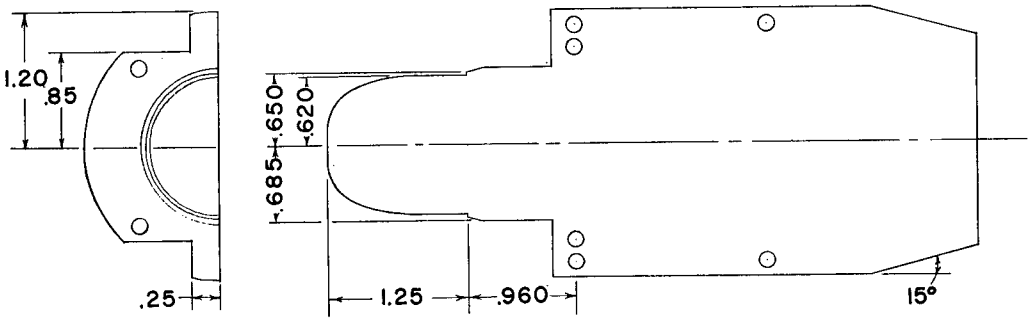

x, in.	y, in.
.0000	.6200
.0500	.4501
.1500	.3282
.3000	.2188
.4500	.1448
.6500	.0767
.8500	.0329
1.0500	.0081
1.2500	.0000

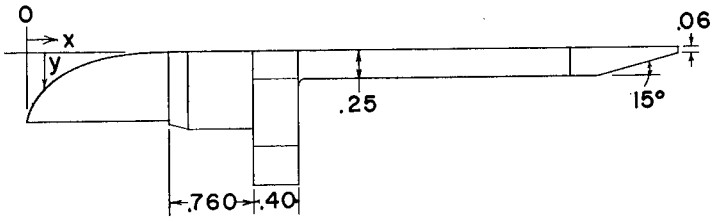

(b) Flat plate.

Figure 4.- General arrangement of the semicircular nozzles. All dimensions are in inches.

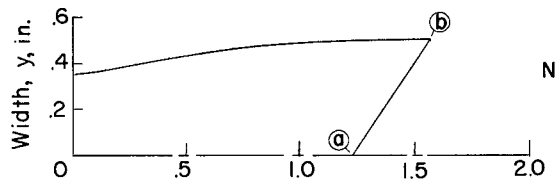

Nozzle 1

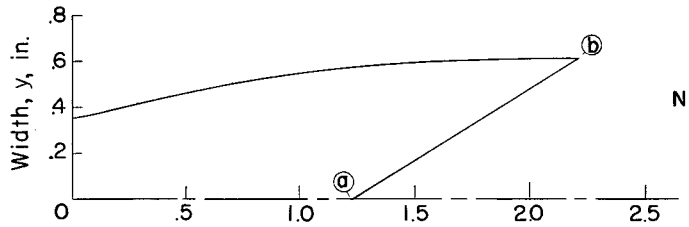

Nozzle 2

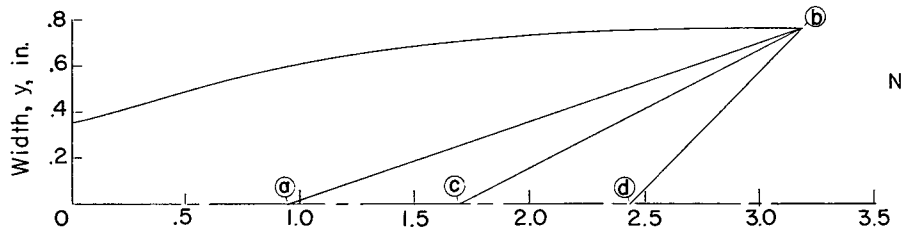

Nozzle 3

Nozzle	Mach no.	Notch	Point	x, in.	y, in.
1	2.22	1/3	a	1.228	0
			b	1.563	.504
2	2.63	2/3	a	1.226	0
			b	2.216	.611
3	3.10	3/3	a	.952	0
			b	3.183	.761
		2/3	c	1.696	0
		1/3	d	2.439	0
4	3.41	ΔM=5% M=3.24	a	1.030	0
			b	1.050	.06
			c	1.200	.15
			d	2.790	.856
		3/3	e	1.122	0
			f	4.005	.884
		2/3	g	2.083	0
		1/3	h	3.044	0

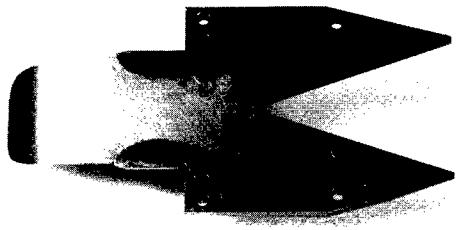

Flat plate with V—notch

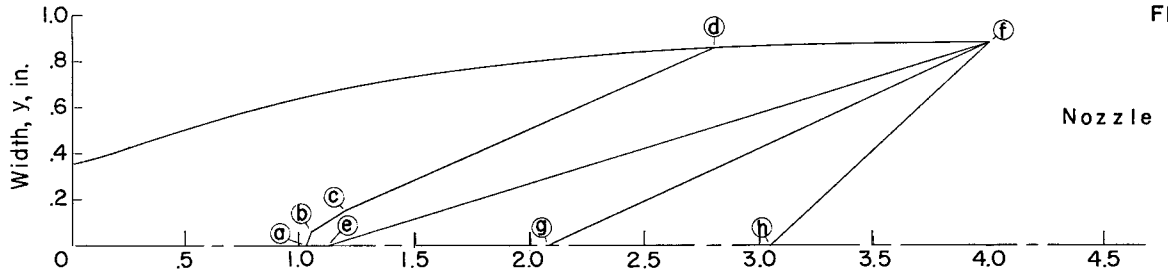

Nozzle 4

Nozzle center-line length from throat, x, in.

Figure 5.- Flat plate with V-notches (semiplan).

L-64-7904

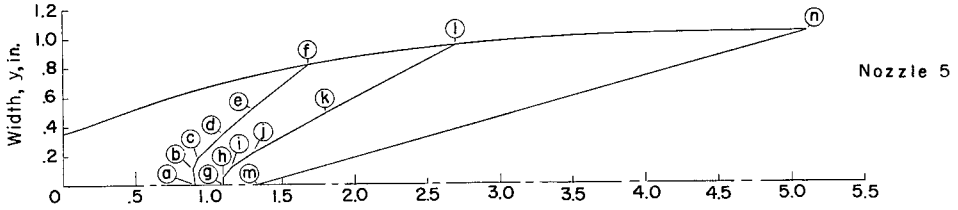

Nozzle 5

Nozzle	Mach no.	Notch	Point	x, in.	y, in.
5	3.76	ΔM=20% M=3.01	a	.905	0
			b	.890	.11
			c	.920	.18
			d	1.100	.35
			e	1.300	.525
			f	1.680	.82
		ΔM=10% M=3.38	g	1.095	0
			h	1.095	.05
			i	1.150	.12
			j	1.300	.22
			k	1.800	.49
			l	2.690	.953
		3/3	m	1.333	0
			n	5.108	1.039
6	4.02	ΔM=10% M=3.62	a	1.250	0
			b	1.260	.09
			c	1.400	.19
			d	1.900	.45
			e	3.170	1.073
		3/3	f	1.502	0
			g	6.059	1.169
		2/3	h	3.021	0
		1/3	i	4.540	0
7	4.54	ΔM=30% M=3.18	a	.995	0
			b	.970	.22
			c	1.100	.395
			d	1.590	.90
		ΔM=20% M=3.63	e	1.250	0
			f	1.280	.15
			g	1.350	.27
			h	1.700	.52
			i	2.700	1.14
		ΔM=10% M=4.09	j	1.545	0
			k	1.600	.09
			l	1.700	.18
			m	1.900	.29
			n	2.700	.64
			o	4.400	1.33
		3/3	p	1.874	0
			q	8.350	1.462

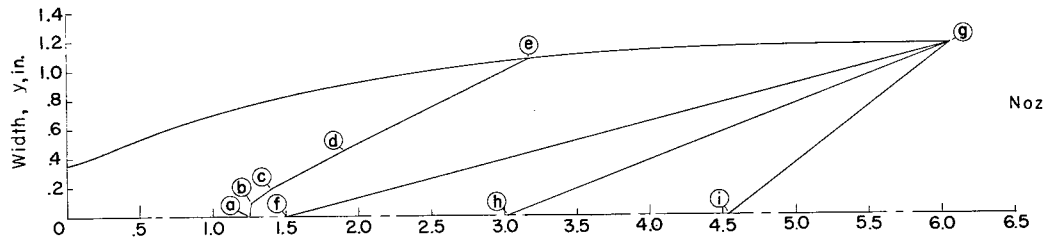

Nozzle 6

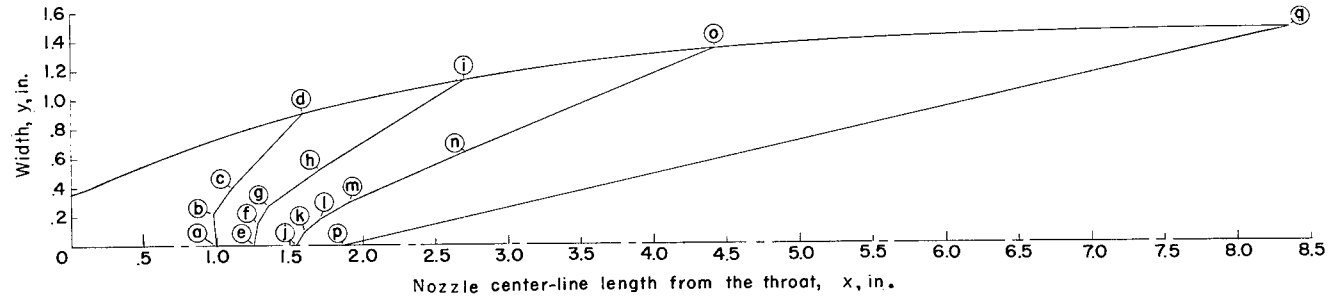

Nozzle 7

Figure 5.- Concluded.

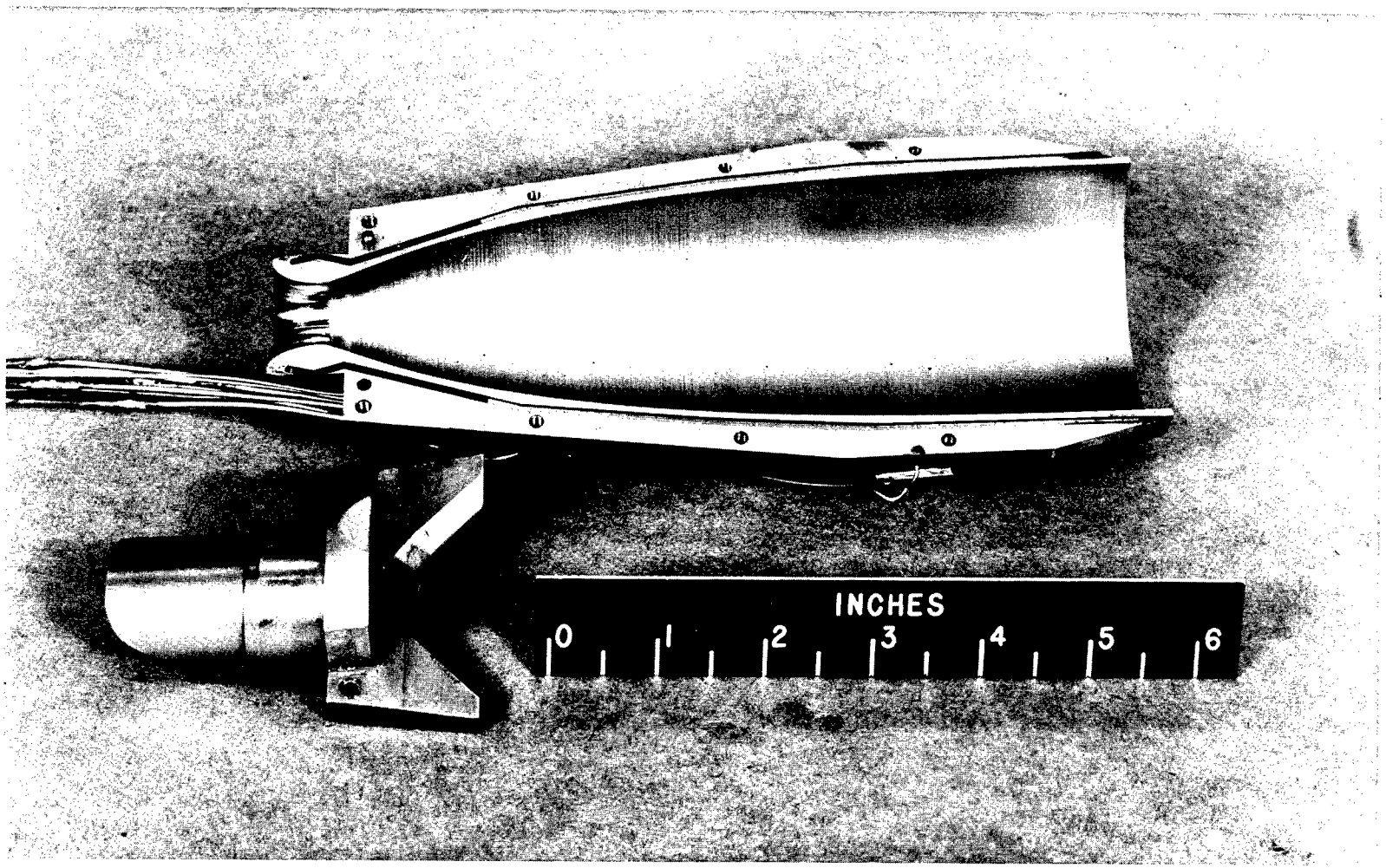

Figure 6.- Nozzle 7 with the largest notch (ΔM = 30 percent). L-63-5445

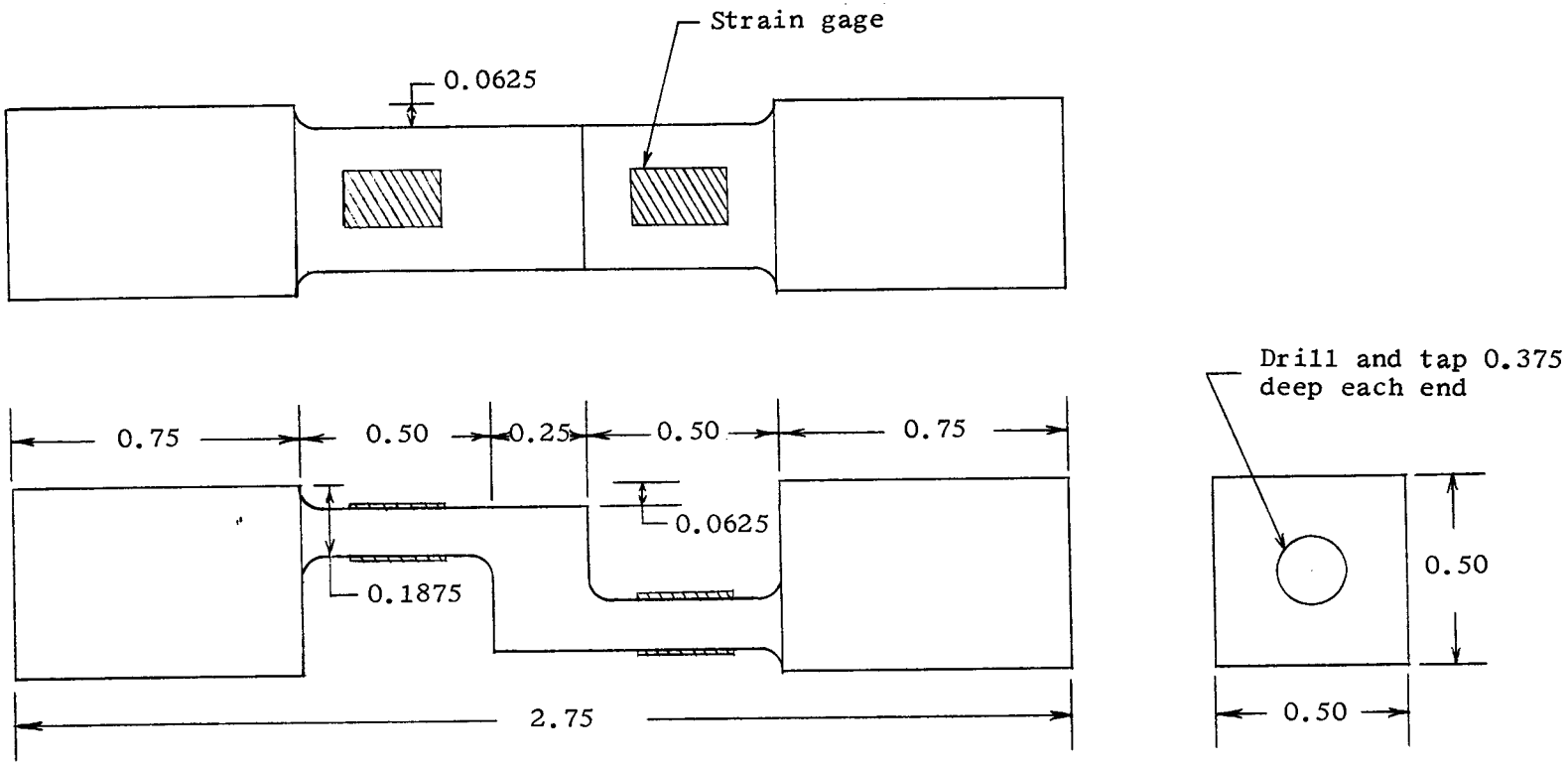

Figure 7.- Tension beam used to indicate lift. All dimensions are in inches; maximum load, 100 lb.

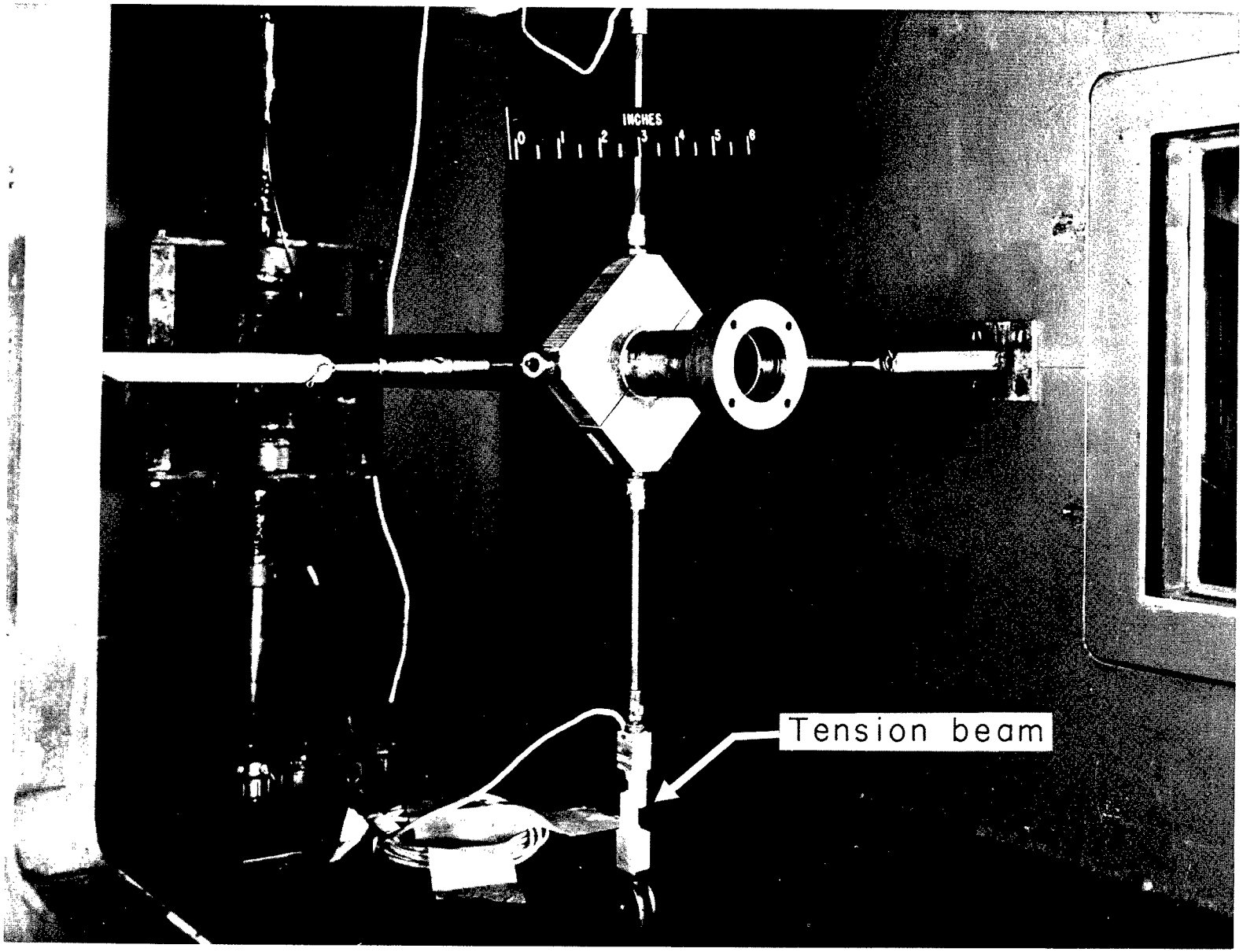

Figure 8.- Method of mounting tension beams in test section. L-63-5447.1

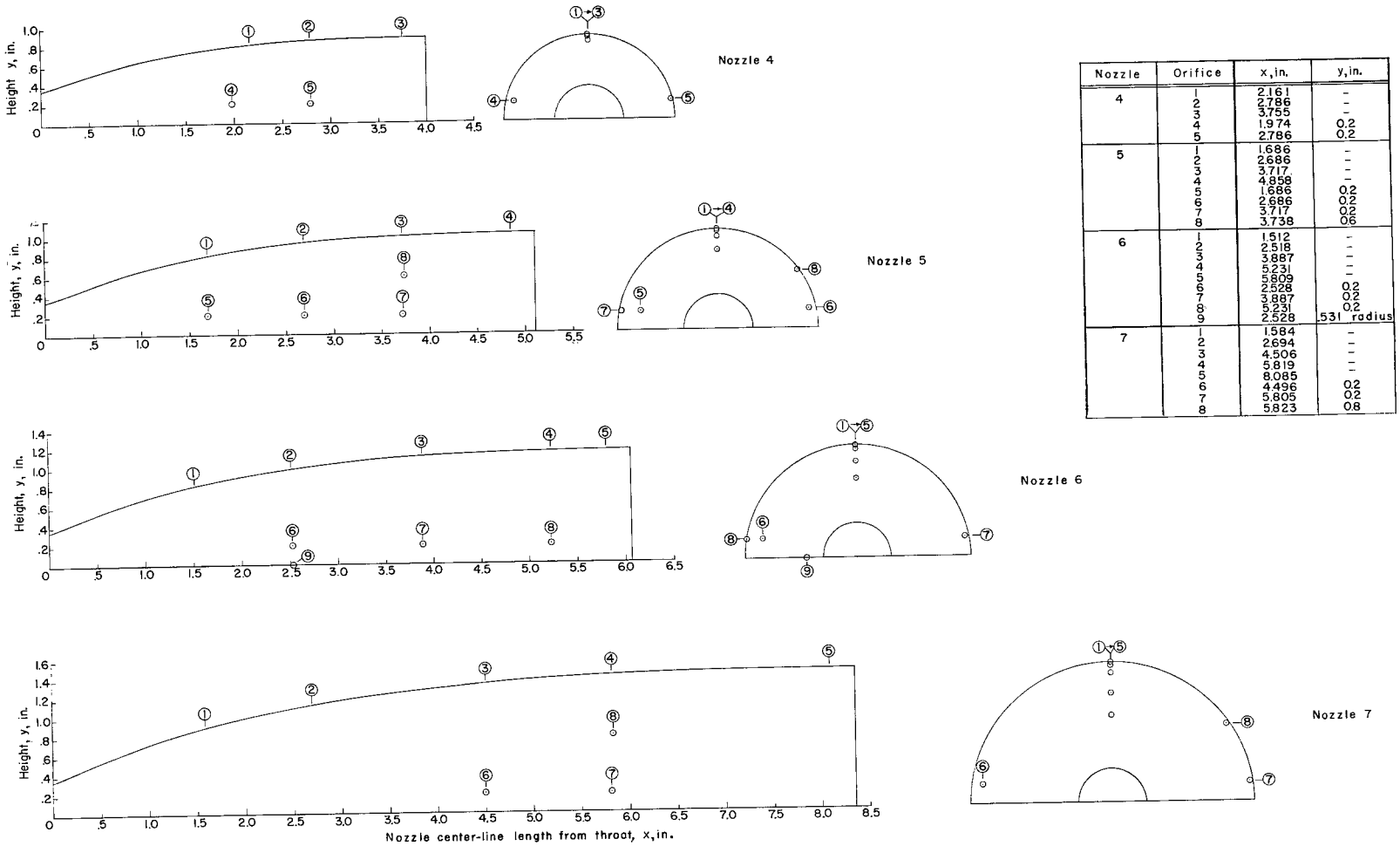

Nozzle	Orifice	x, in.	y, in.
4	1	2.161	-
	2	2.786	-
	3	3.755	-
	4	1.974	0.2
	5	2.786	0.2
5	1	1.686	-
	2	2.686	-
	3	3.717	-
	4	4.858	-
	5	1.686	0.2
	6	2.686	0.2
	7	3.717	0.2
	8	3.738	0.6
6	1	1.512	-
	2	2.518	-
	3	3.887	-
	4	5.231	-
	5	5.809	-
	6	2.528	0.2
	7	3.887	0.2
	8	5.231	0.2
	9	2.528	.531 radius
7	1	1.584	-
	2	2.694	-
	3	4.506	-
	4	5.819	-
	5	8.085	-
	6	4.496	0.2
	7	5.805	0.2
	8	5.823	0.8

Figure 9.- Static orifice locations on the nozzle internal surface.

Circular nozzle

Nozzle 1, M = 2.22

Symbol	$p_{\infty,av}$, psia
○	8.1
□	2.2
◇	0.7

– – – – inviscid C_T

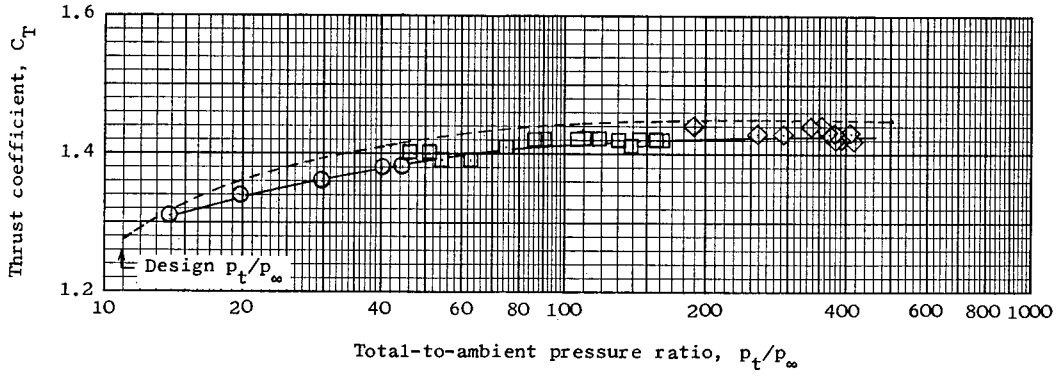

Circular nozzle

Nozzle 2, M = 2.63

Symbol	$p_{\infty,av}$, psia
○	7.8
□	1.9
◇	0.6

– – – – inviscid C_T

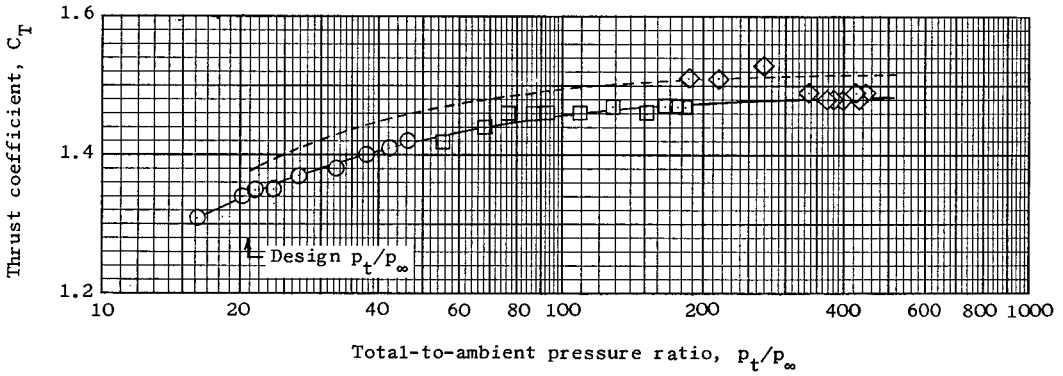

Circular nozzle

Nozzle 3, M = 3.10

Symbol	$p_{\infty,av}$, psia
○	4.3
□	2.3
◇	0.6

– – – – inviscid C_T

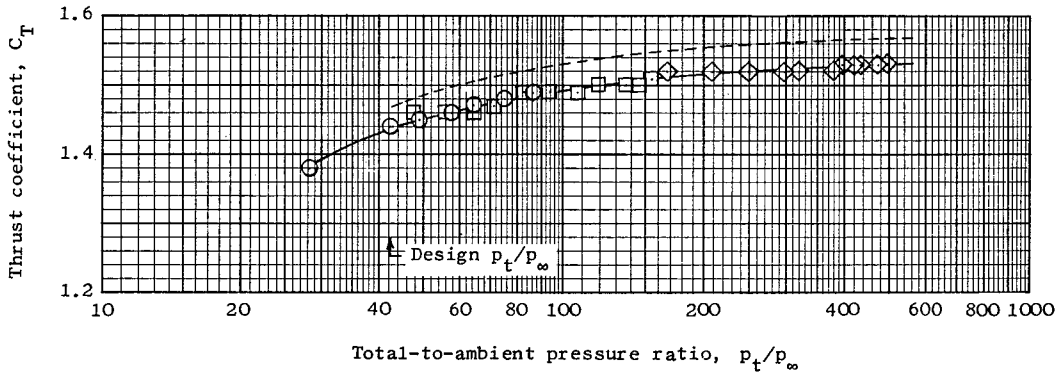

Figure 10.- Circular nozzle thrust coefficient.

Circular nozzle

Nozzle 4, M = 3.41

Symbol	$p_{\infty,av}$, psia
○	4.0
□	4.0
◇	2.0
△	1.9
◺	0.5

– – – – inviscid C_T

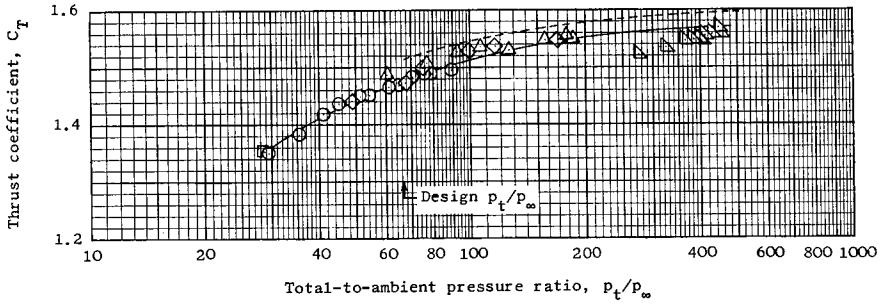

Circular nozzle

Nozzle 5, M = 3.76

Symbol	$p_{\infty,av}$, psia
○	2.1
□	1.0
◇	0.6

– – – – inviscid C_T

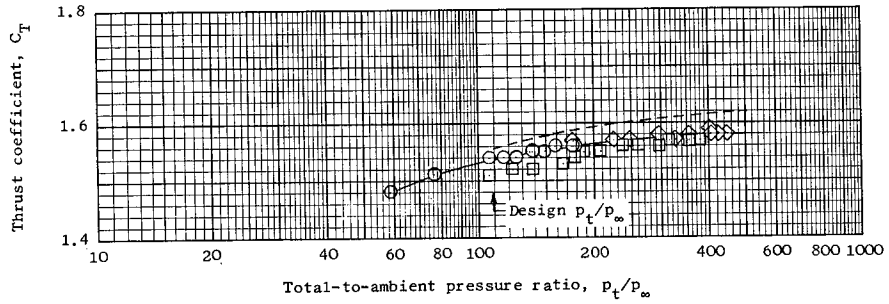

Circular nozzle

Nozzle 6, M = 4.02

Symbol	$p_{\infty,av}$, psia
○	1.5
□	1.1
◇	0.6

– – – – inviscid C_T

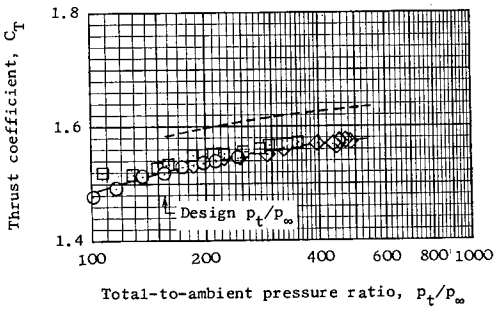

Circular nozzle

Nozzle 7, M = 4.54

Symbol	$p_{\infty,av}$, psia
○	1.0
□	0.7
◇	0.6

– – – – inviscid C_T

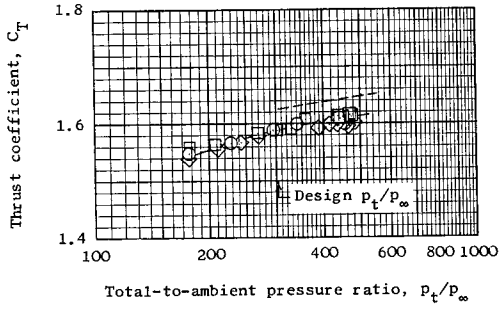

Figure 10.- Concluded.

Semicircular nozzle

Nozzle 1, M = 2.22

Symbol	$p_{\infty,av}$, psia
○	8.5
□	2.1
◇	0.7

– – – – inviscid C_T

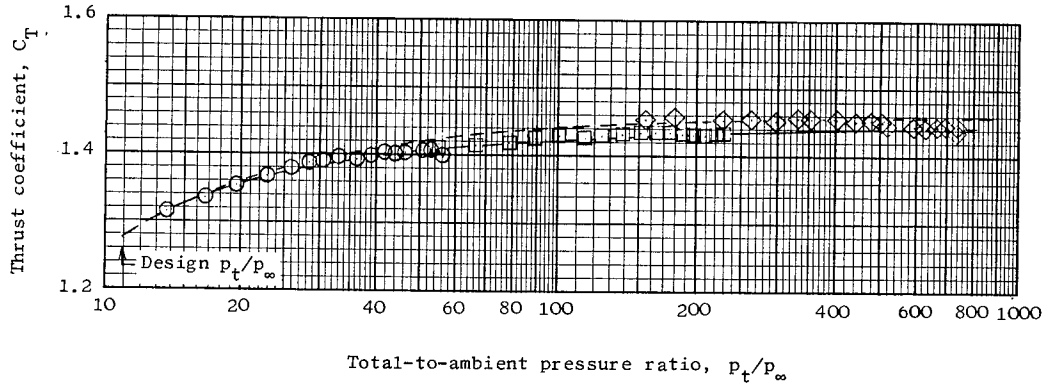

Semicircular nozzle

Nozzle 2, M = 2.63

Symbol	$p_{\infty,av}$, psia
○	2.1
□	0.4

– – – – inviscid C_T

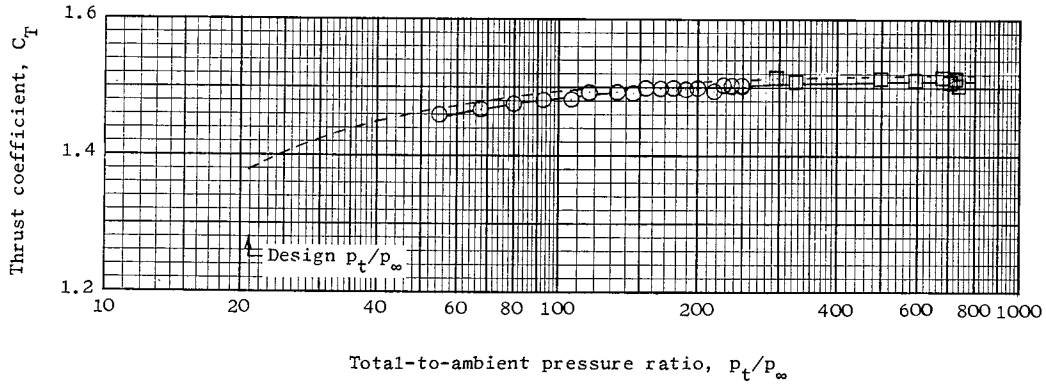

Semicircular nozzle

Nozzle 3, M = 3.10

Symbol	$p_{\infty,av}$, psia
○	1.9
□	0.3

– – – – inviscid C_T

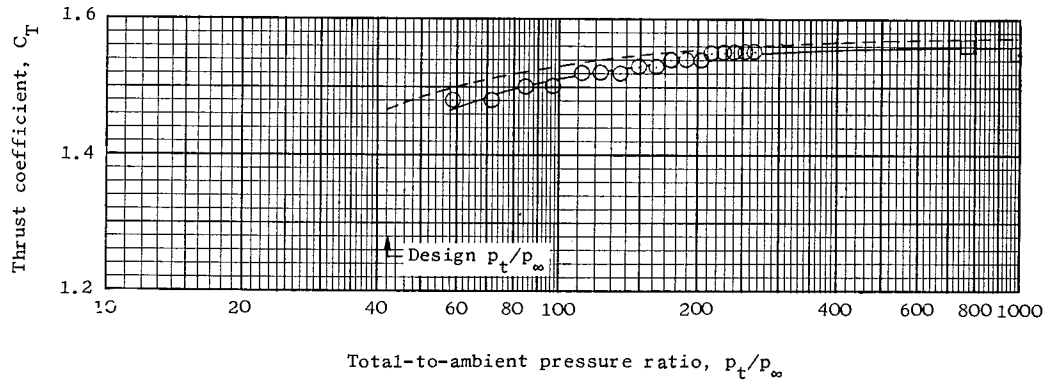

Figure 11.- Thrust coefficient of semicircular nozzle with solid flat plate.

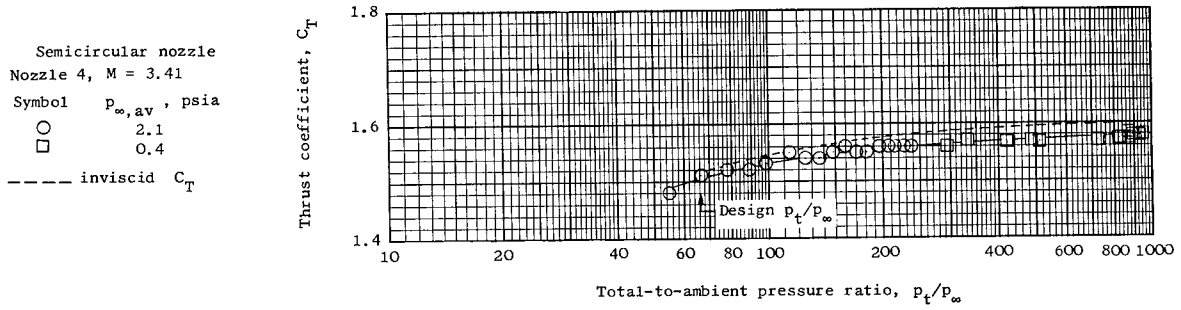

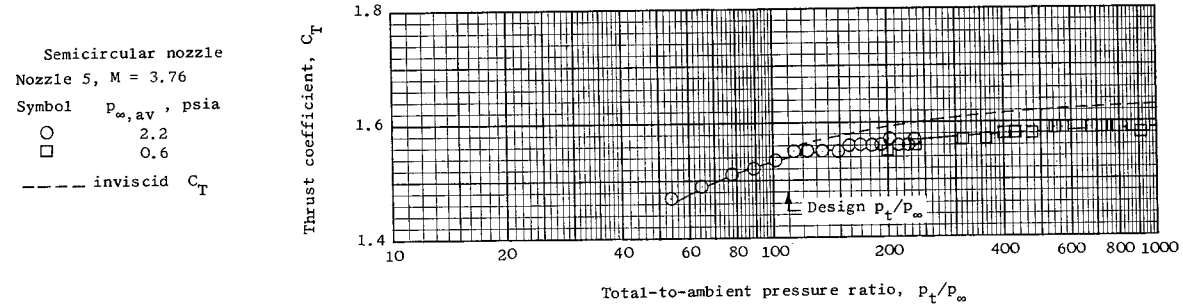

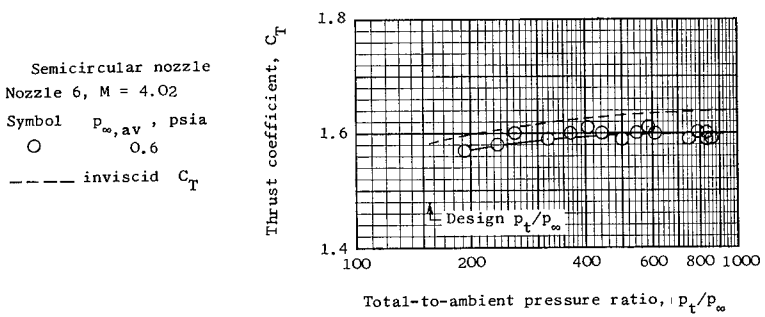

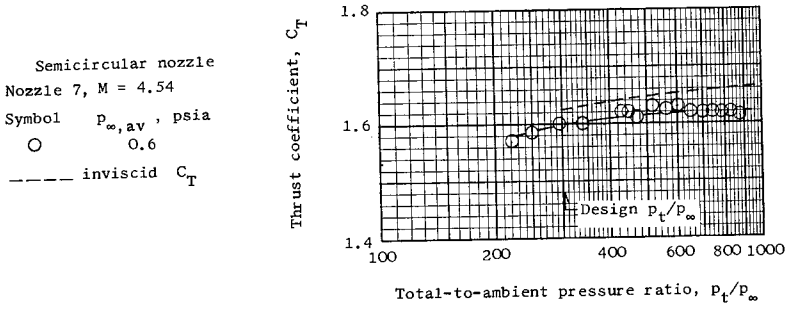

Figure 11.- Concluded.

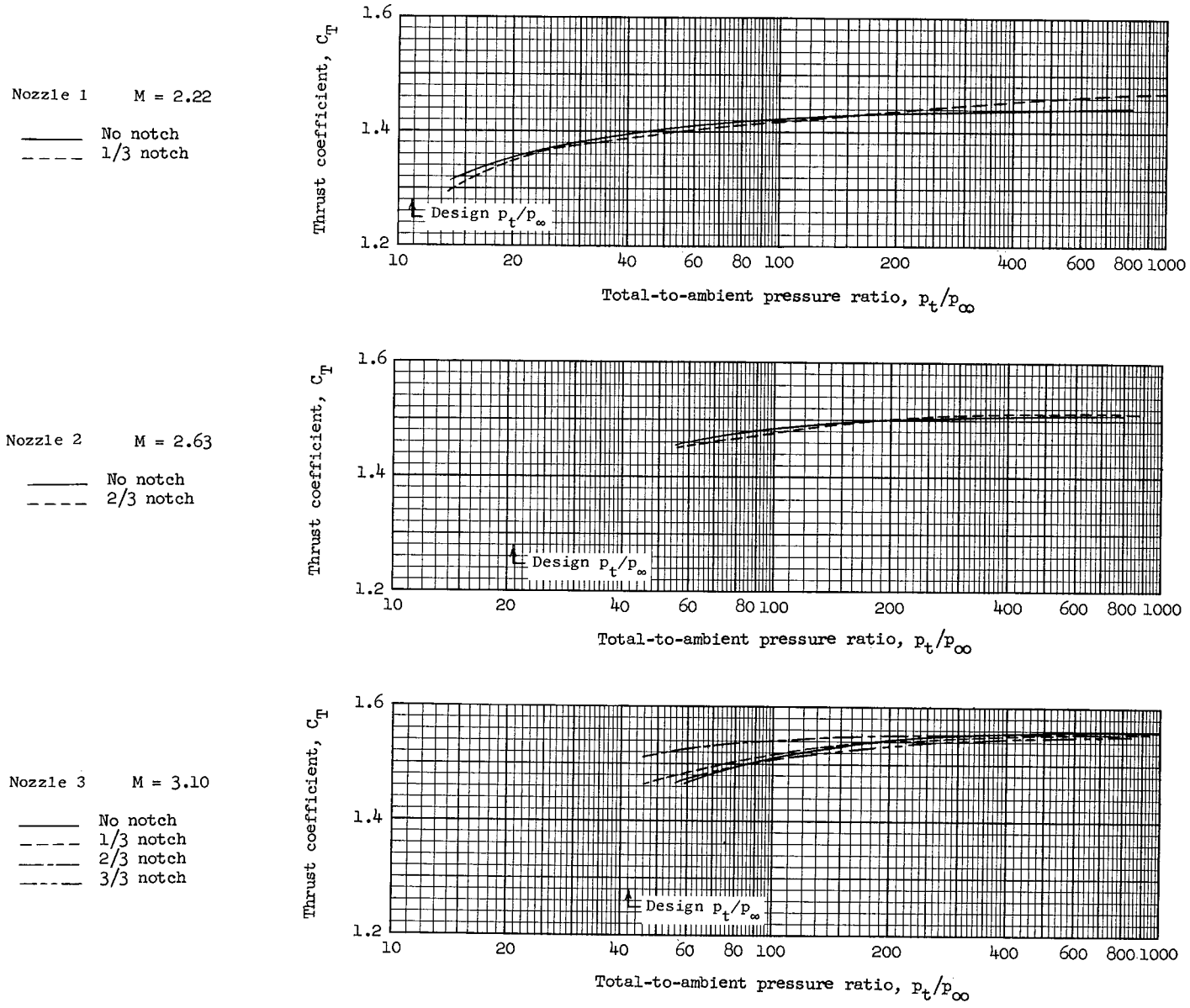

Figure 12.- Faired values of the thrust coefficients for the semicircular nozzles.

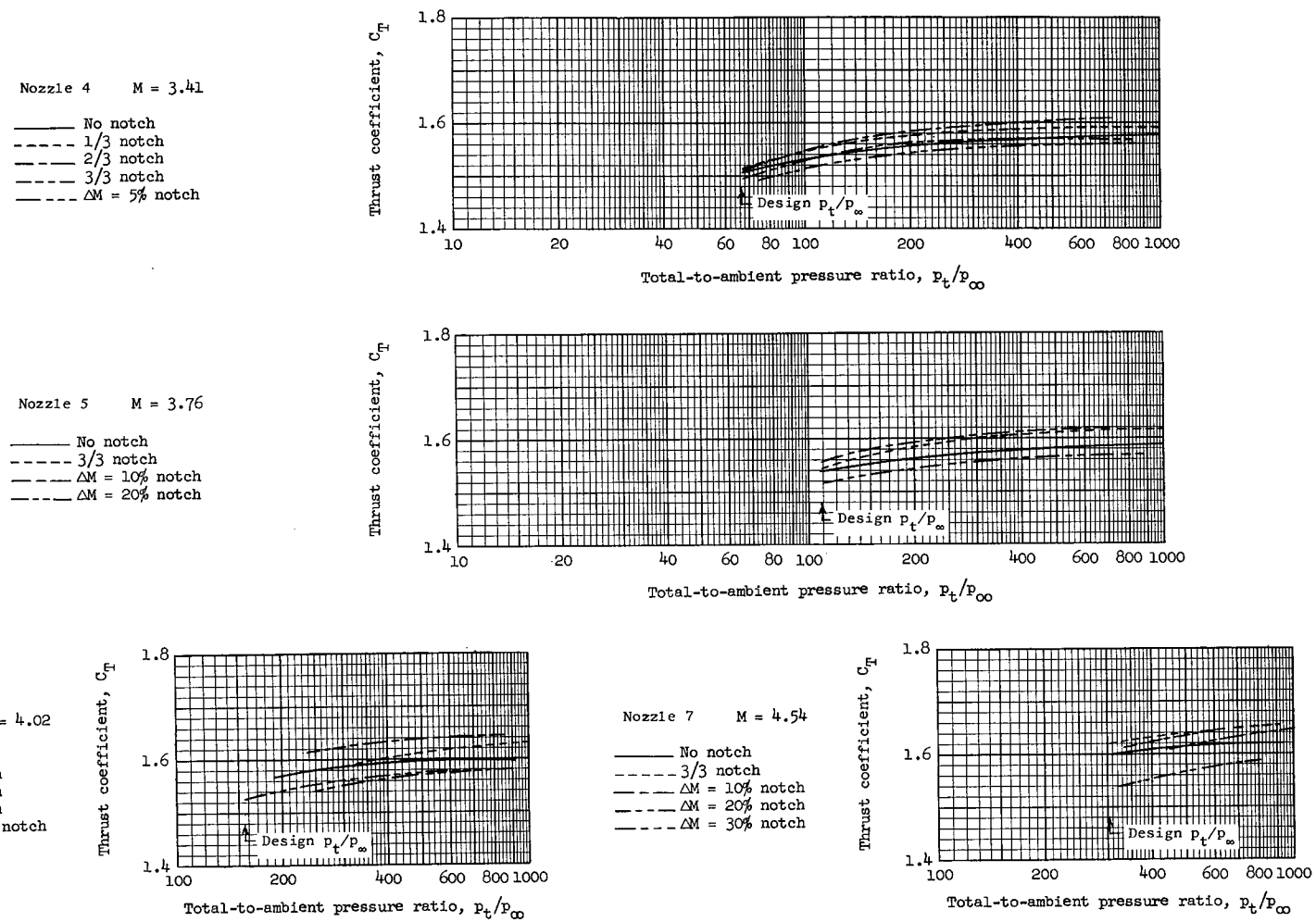

Figure 12.- Concluded.

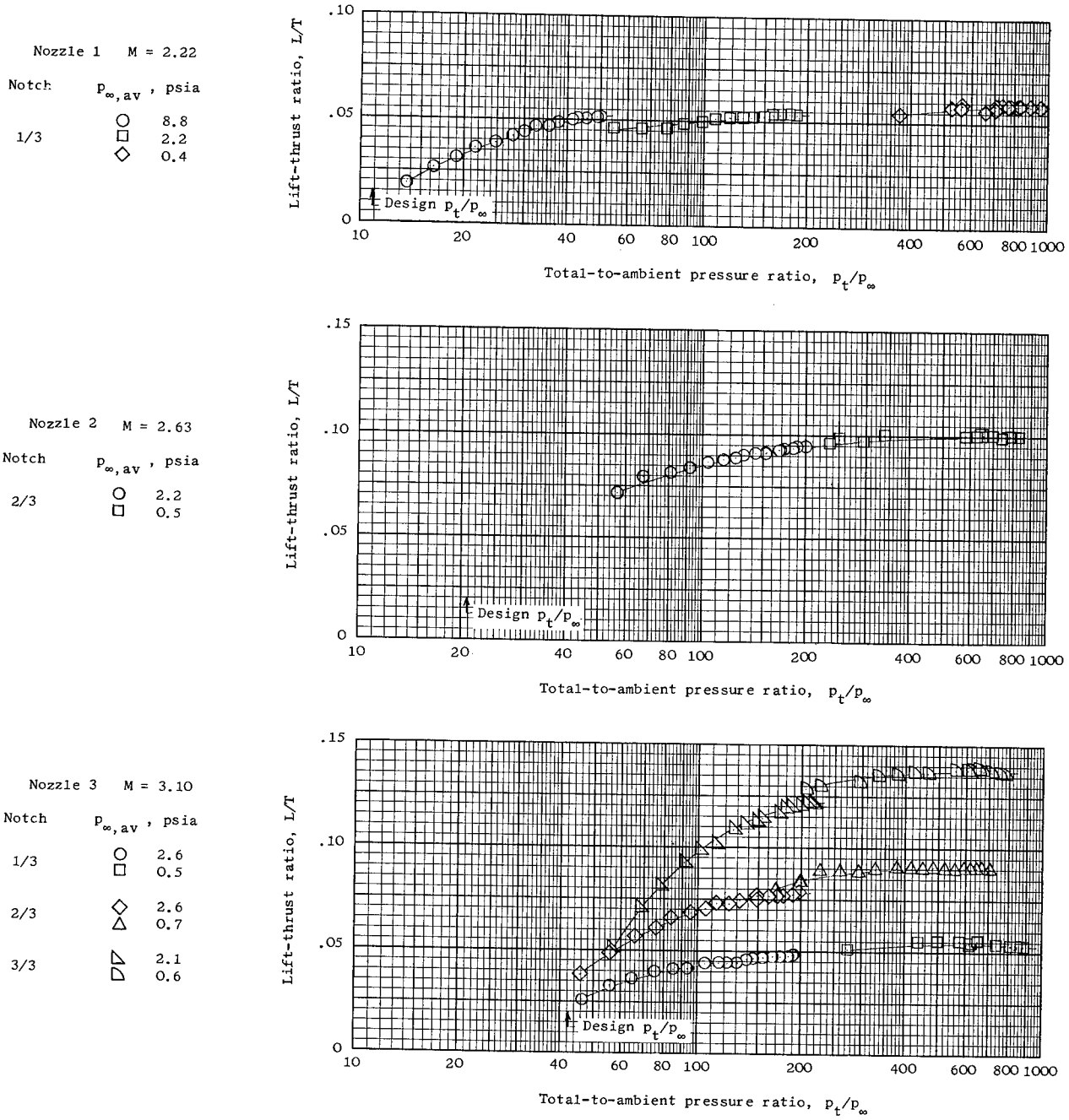

Figure 13.- Lift-thrust ratio of the lift-producing nozzles.

Nozzle 4 M = 3.41

Notch	$p_{\infty,av}$, psia
1/3	2.0
	0.4
2/3	2.2
	0.5
3/3	2.1
	0.5
ΔM = 5%	2.3
	0.6

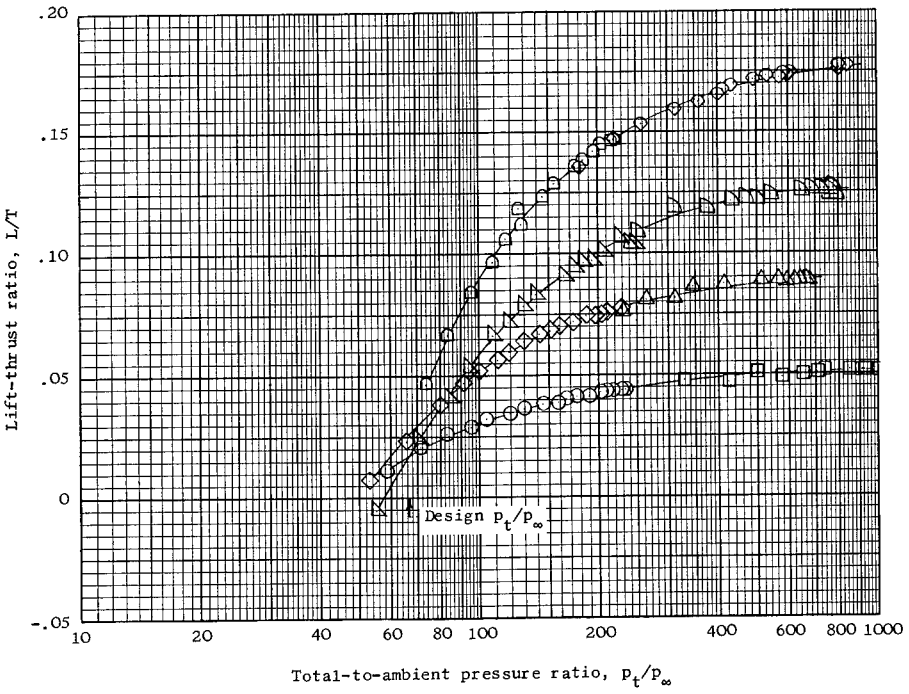

Nozzle 5 M = 3.76

Notch	$p_{\infty,av}$, psia
3/3	2.1
	0.4
ΔM = 10%	2.3
	0.6
ΔM = 20%	2.0
	0.5

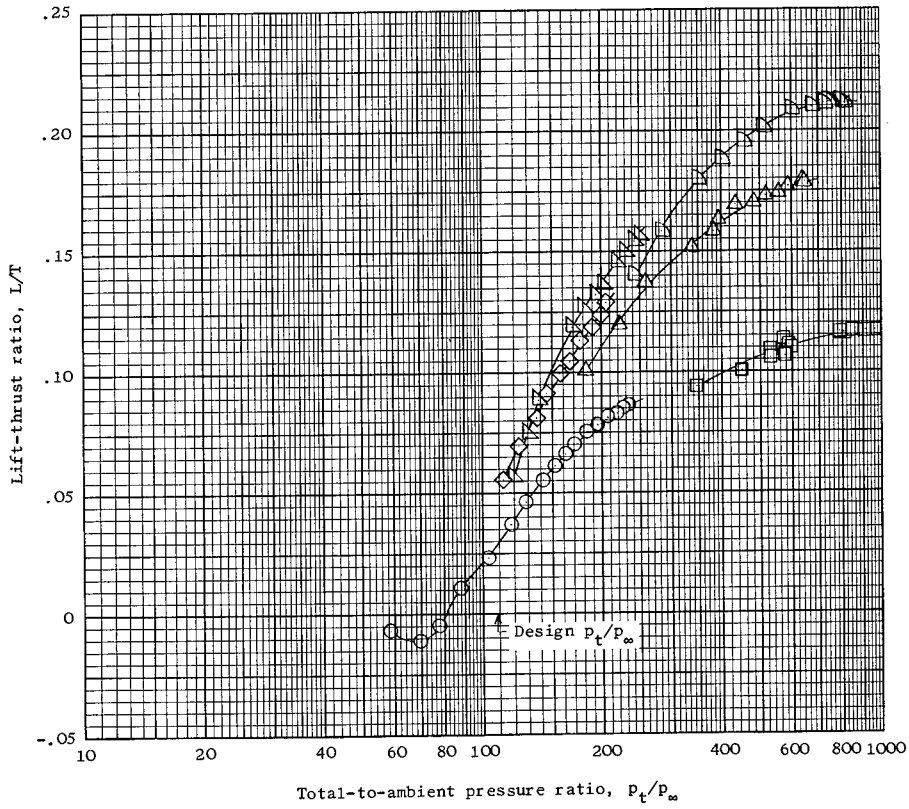

Figure 13.- Continued.

Nozzle 6 M = 4.02

Notch		$p_{\infty,av}$, psia
1/3	○	0.4
2/3	□	0.5
3/3	◇	0.5
ΔM = 10%	△	0.7

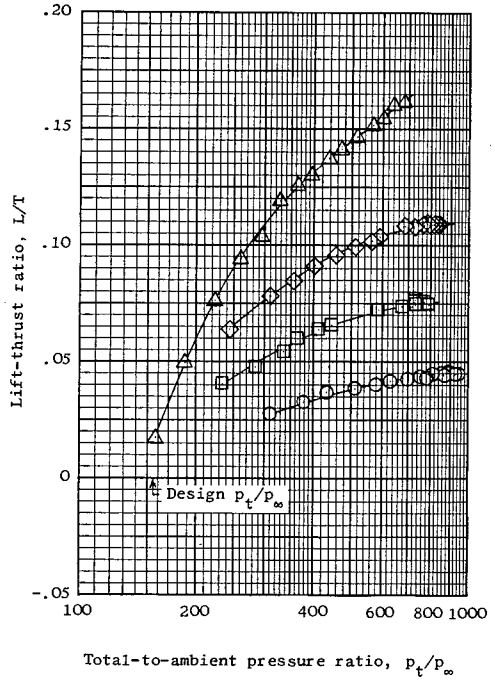

Nozzle 7 M = 4.54

Notch		$p_{\infty,av}$, psia
3/3	○	0.5
ΔM = 10%	□	0.6
ΔM = 20%	◇	0.7
ΔM = 30%	△	0.4

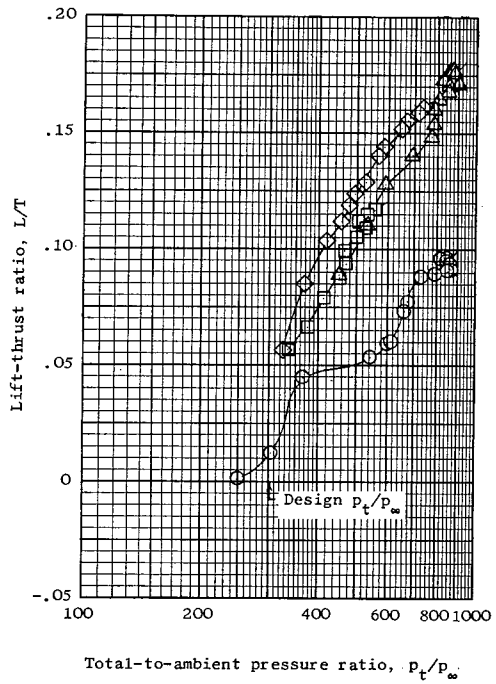

Figure 13.- Concluded.

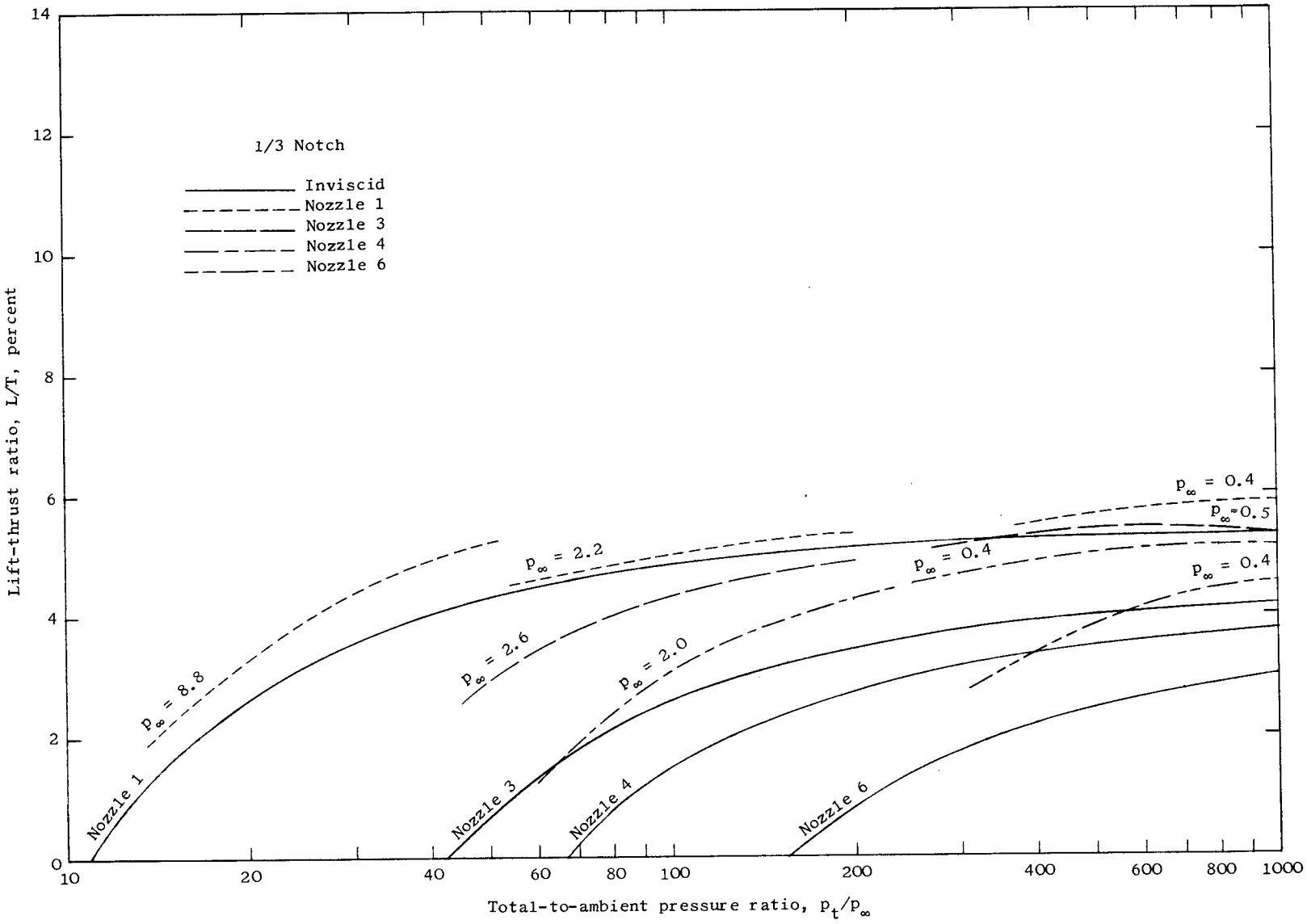

Figure 14.- Comparison of inviscid and experimental lift-thrust ratios for the V-notches.

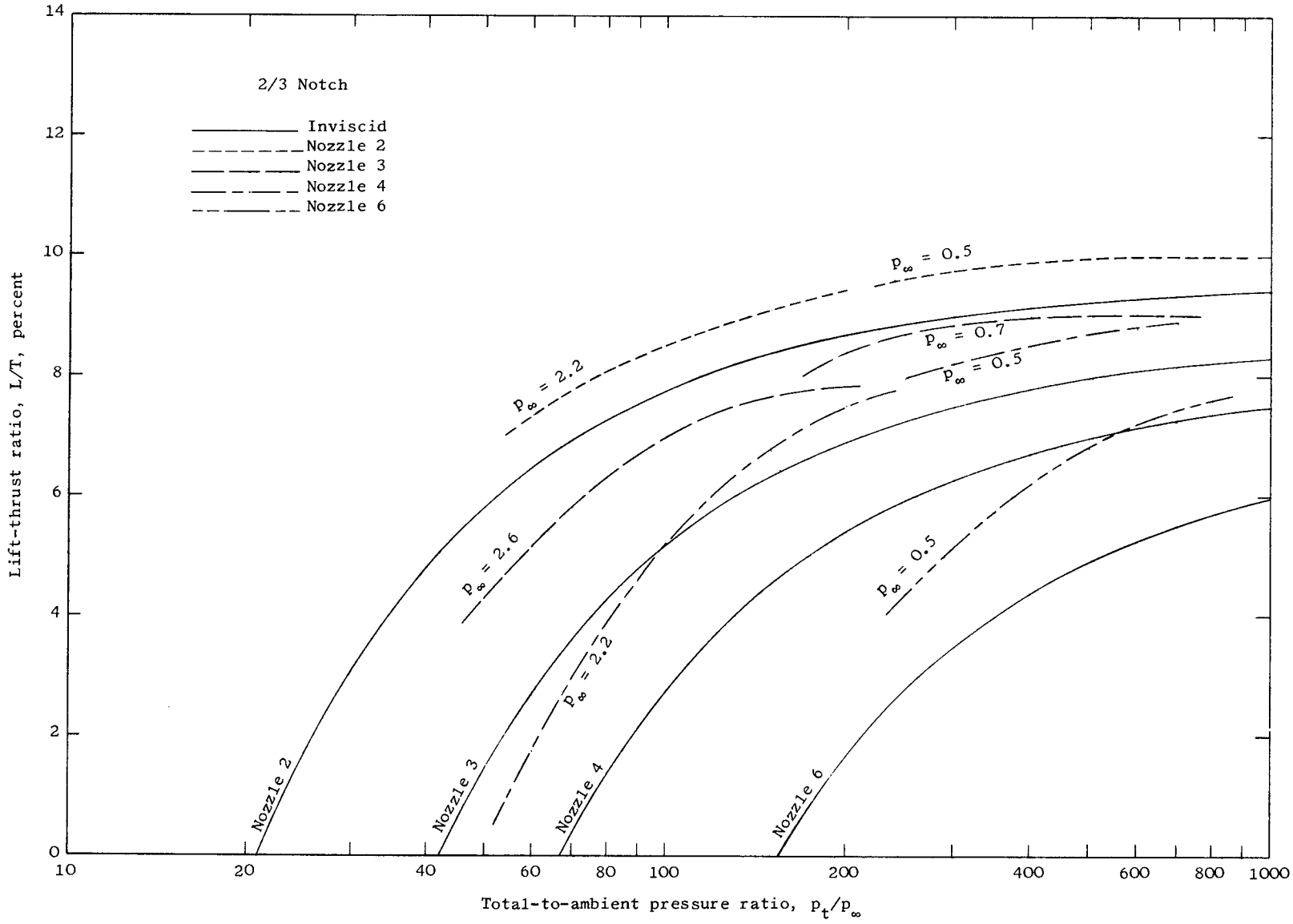

Figure 14.- Continued.

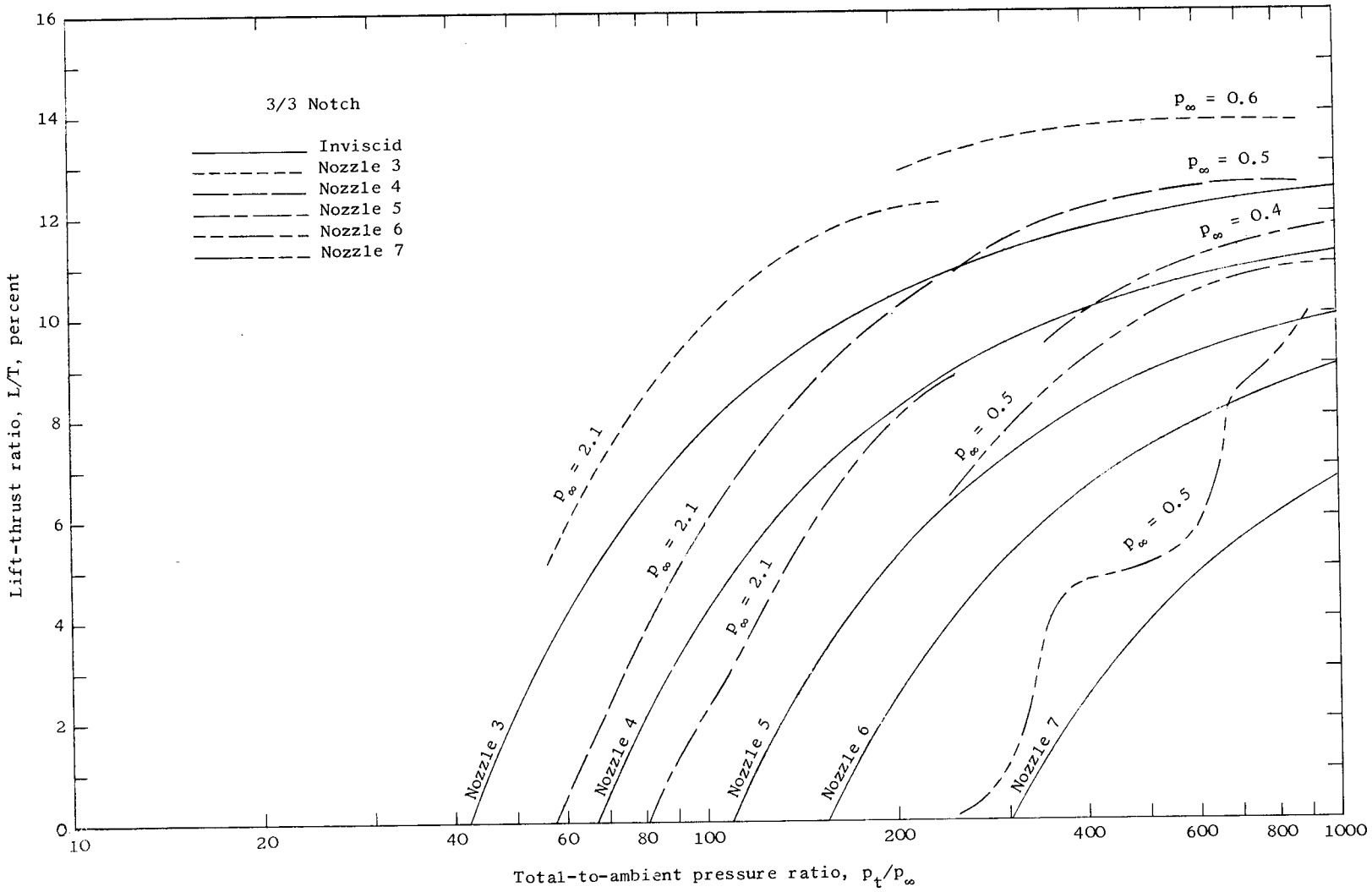

Figure 14.- Concluded.

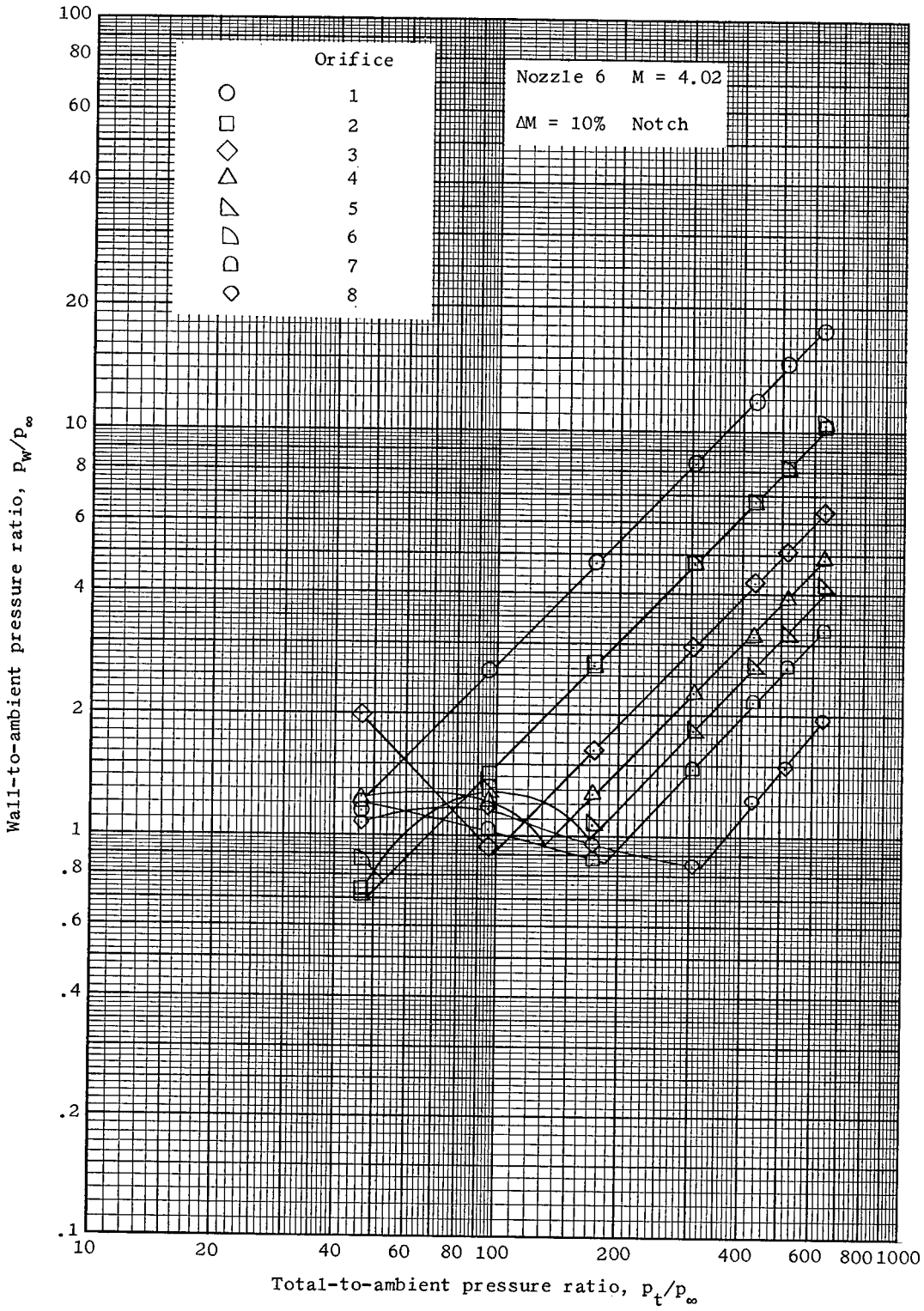

Figure 15.- Example of plot used to determine separation pressure.

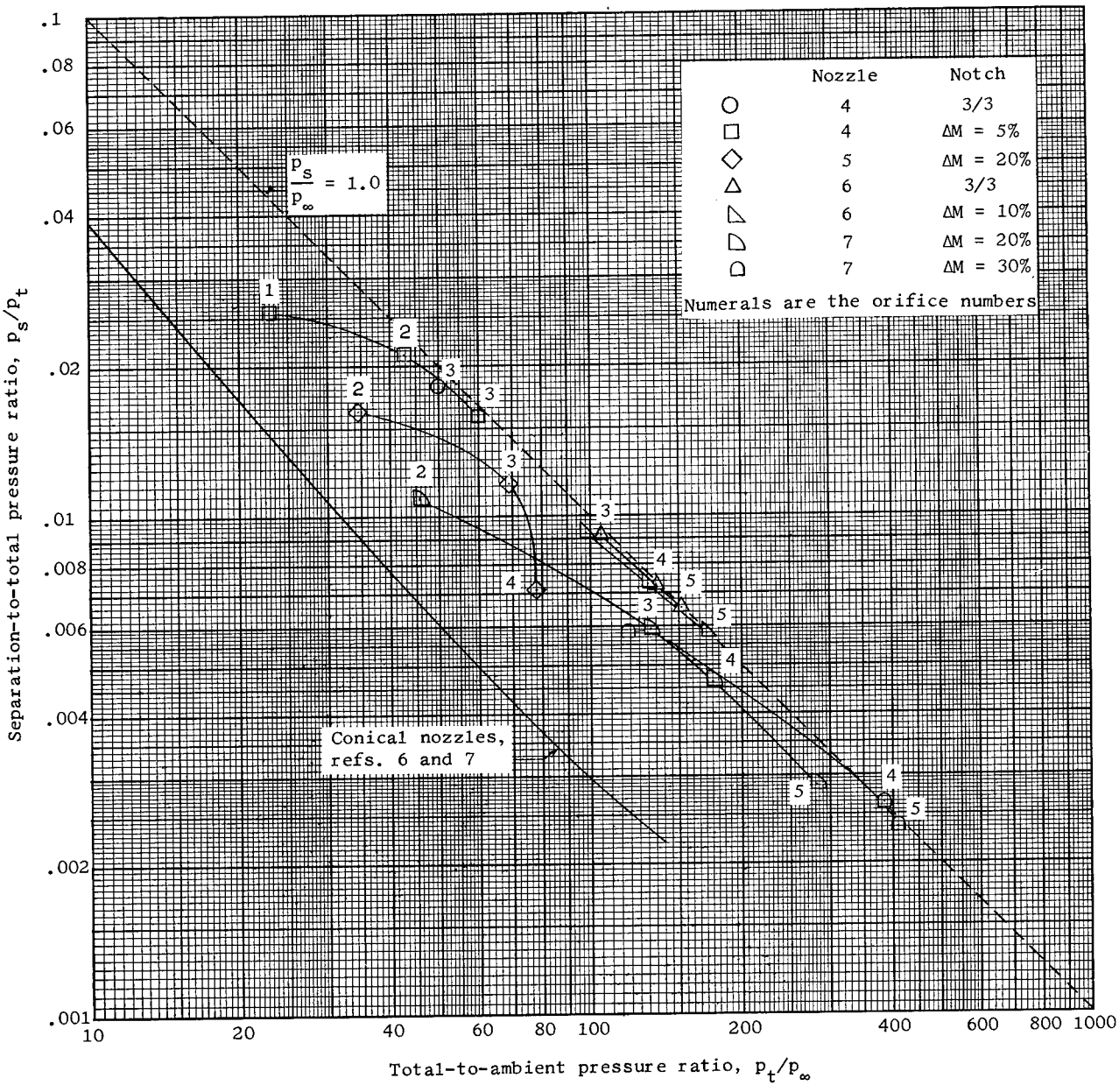

(a) Separation pressure on top center line of nozzle.

Figure 16.- Separation pressure of semicircular nozzle with notched flat plate.

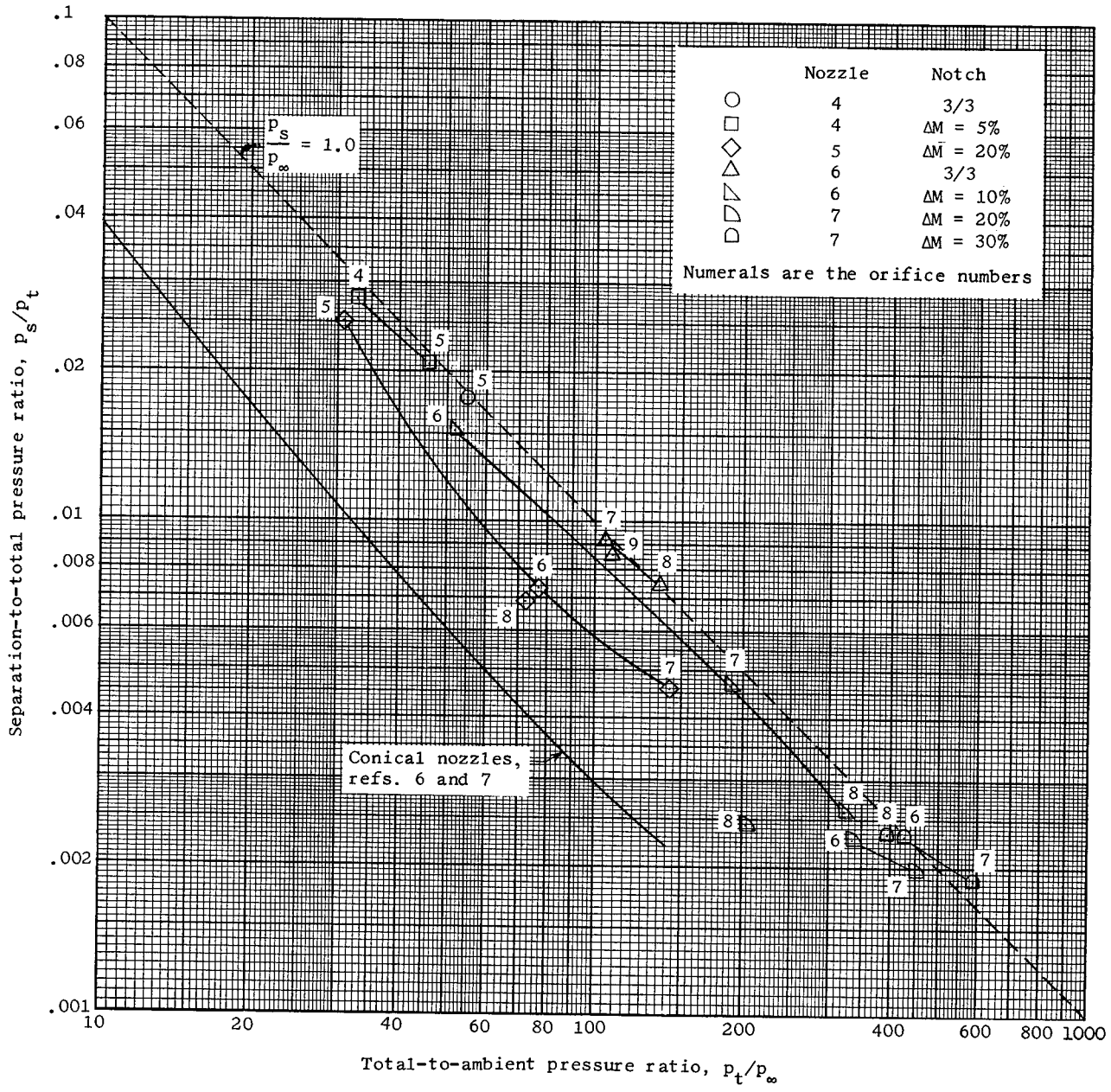

(b) Separation pressure not on top center line of nozzle.

Figure 16.- Concluded.

Circular configuration

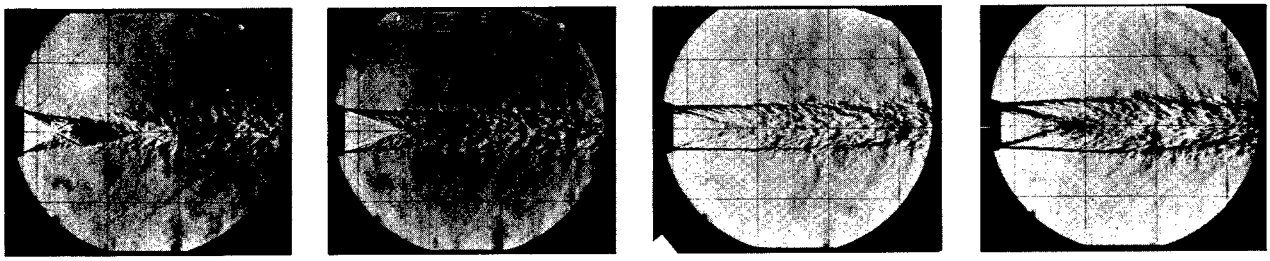

$\frac{p_t}{p_\infty} = 25.3$ $\frac{p_t}{p_\infty} = 48.8$ $\frac{p_t}{p_\infty} = 75.0$ $\frac{p_t}{p_\infty} = 99.7$

Semicircular configuration solid flat plate

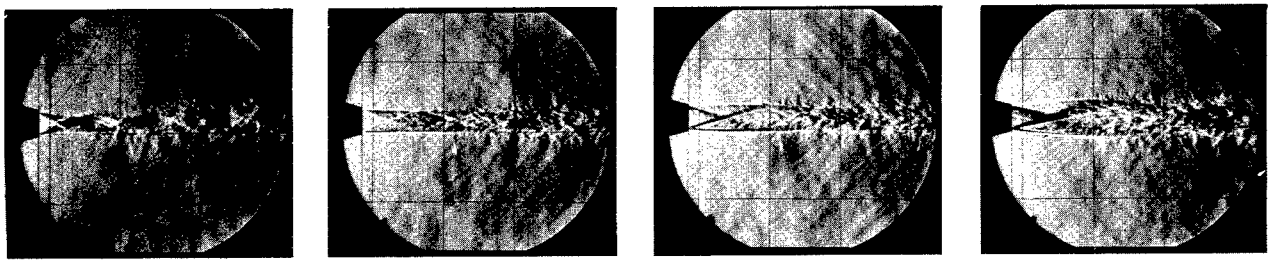

$\frac{p_t}{p_\infty} = 27.3$ $\frac{p_t}{p_\infty} = 48.8$ $\frac{p_t}{p_\infty} = 75.1$ $\frac{p_t}{p_\infty} = 105.7$

Semicircular configuration $\frac{3}{3}$ notch

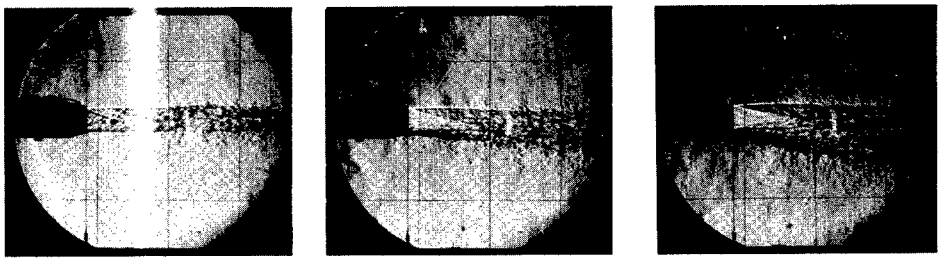

$\frac{p_t}{p_\infty} = 55.1$ $\frac{p_t}{p_\infty} = 87.9$ $\frac{p_t}{p_\infty} = 118.4$

(a) Nozzle 4; design $\frac{p_t}{p_\infty} = 66.8$. L-64-10210

Figure 17.- Schlieren photographs. Vertical knife edge.

Semicircular configuration ΔM = 10% notch

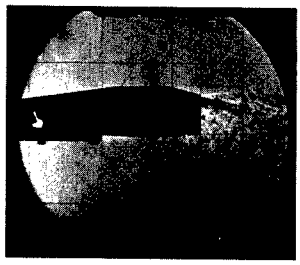

$\frac{p_t}{p_\infty}$ = 129.6

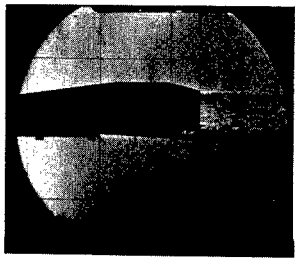

$\frac{p_t}{p_\infty}$ = 359.9

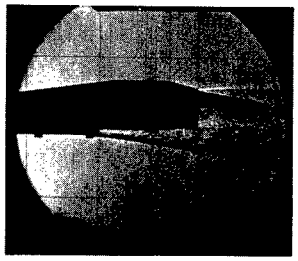

$\frac{p_t}{p_\infty}$ = 563.3

Semicircular configuration ΔM = 30% notch

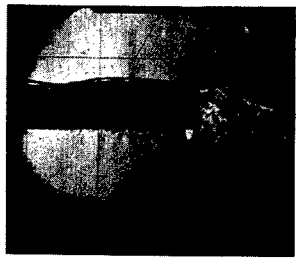

$\frac{p_t}{p_\infty}$ = 116.7

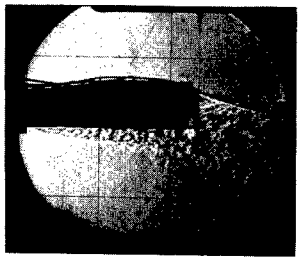

$\frac{p_t}{p_\infty}$ = 283.7

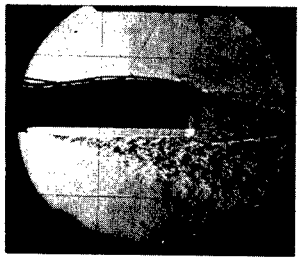

$\frac{p_t}{p_\infty}$ = 623.3

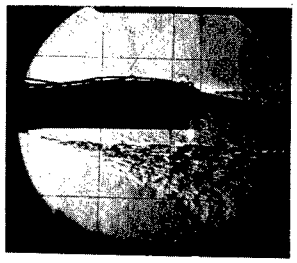

$\frac{p_t}{p_\infty}$ = 791.9

(b) Nozzle 7; design $\frac{p_t}{p_\infty}$ = 301.3. L-64-10211

Figure 17.- Concluded.

NASA-Langley, 1965 L-3758